UCRL-TR-202775

Screening of Maritime Containers to Intercept Weapons of Mass Destruction

Arden Dougan, Dennis Slaughter, Mark Accatino, Ken Sale, Owen Alford, Adam Bernstein, Marie-Anne Descalle, Dan Dietrich, Mike Frank, C. Hagmann, Howard Hall, Dale Hankins, Dave Johnson, James Hall, Alex Loshak, John Luke, Doug Manatt, Gary Mattesich, Joe Mauger, Robin Newmark, Bert Pohl, Stanley Prussin (UC Berkeley), Mark Rowland, Tom Schaffer, Brad Sleaford, Jerry Stengel, Dave Trombino, Rosemary Walling, David Weirup, Jim Wolford.

February 2004

This work was performed under the auspices of the U.S. Department of Energy by University of California, Lawrence Livermore National Laboratory under Contract W-7405-Eng-48.

Summary

The goal of our research was to address the problem of detection of weapons of mass destruction (WMD) materials within containers in common use on commercial cargo trafficking. LLNL has created an experimental test bed for researching potential solutions using (among other techniques) active interrogation with neutrons. Experiments and computational modeling were used to determine the effectiveness of the technique.

Chemical weapons materials and high explosives can be detected using neutron activation and simple geometries with little or no intervening material. However in a loaded container there will be nuisance alarms from conflicting signatures resulting from the presence of material between the target and the detector (and the interrogation source). Identifying some elements may require long counting times because of the increased background. We performed some simple signature measurements and simulations of gamma-ray spectra from several chemical simulants. We identified areas where the nuclear data was inadequate to perform detailed computations.

We concentrated on the detection of SNM in cargo containers, which will be emphasized here. The goal of the work reported here is to develop a concept for an active neutron interrogation system that can detect small targets of SNM contraband in cargo containers, roughly 5 kg HEU or 1 kg Pu, even when well shielded by a thick cargo. It is essential that the concept be reliable and have low false-positive and false-negative error rates. It also must be rapid to avoid interruption of commerce, completing the analysis in minutes.

A potentially viable concept for cargo interrogation has been developed and its components have been evaluated experimentally. A new radiation signature unique to SNM has been identified that utilizes high-energy, fission-product gamma rays. That signature due to β^--radiation in the range 3-6 MeV is distinct from normal background radioactivity that does not extend above 2.6 MeV. It's short half-life of 20-55 sec makes it distinct from neutron activation due to the interrogation that is typically much longer lived. This work spawned a collaboration with LBNL where experiments verified the abundance and other characteristics of this new signature [24]. Follow-on work funded by DoE/NA22 led to the development of a detailed system concept and evaluation of its impact on operating personnel and cargos [60] and characterization of one important interference that was identified [61]. The follow-on work led to two patent applications at LBNL and LLNL. The signature flux, while small, is 2-5 decades more intense than delayed neutron signals used and facilitates the detection of SNM even when shielded by thick cargo. The actual benefit is highly dependent on the type and thickness of cargo, with modest benefit in the case of metallic cargos of iron, lead, or aluminum, but maximum benefit in the case of hydrogenous cargo. In addition, unwanted collateral effects of the interrogation, such as neutron activation of the cargo, were analyzed [60] and one significant interference due to oxygen activation was characterized. This interference can be eliminated by lowering the energy of interrogating neutrons [60] and no others have yet been identified. The neutron source technology required exists commercially.

Follow-on work to produce a laboratory prototype and to engage a commercial partner for development of a prototype to be fielded at a port was

initially funded by DOE/NA-22 is currently supported by DHS. That support is expected to continue through FY06.

Table of Contents

1. Introduction

1.1 Threat description

The largest volume of cargo entering the US is through the shipping ports, which receive about 6 million cargo containers each year. Today approximately 90% of the world's trade moves by cargo containers[1]. Fortunately this traffic is geographically compact where half of all the traffic bound for the US originates in the top ten foreign ports and nearly 90% of the cargo containers arrive here at the top ten US ports of entry, as shown in the table below.

Table 1.1 Ports of origin and ports of entry for US-bound cargo containers[1] in 2001.

Top ten foreign ports of origin			**Top ten domestic ports**		
Port of origin	Number US-bound containers	% of total traffic	**Port of entry**	Number US-bound containers	% of total traffic
Hong Kong	558,600	9.8	Los Angeles	1,774,000	24.7
Shanghai	330,600	5.8	Long Beach	1,371,000	19.1
Singapore	330,600	5.8	New York, New Jersey	1,044,000	14.6
Kaohsiung, Taiwan	319,200	5.6	Charleston	376,000	5.2
Rotterdam	290,700	5.1	Savannah	312,000	4.3
Pusan, South Korea	285,000	5.0	Norfolk	306,000	4.3
Bremerhaven	256,500	4.5	Seattle	284,000	4.0
Tokyo	159,600	2.8	Tacoma	273,000	3.8
Genoa	119,700	2.1	Oakland	268,000	3.7
Yantian, China	114,000	2.0	Houston	233,000	3.3
Top ten total	**2,764,500**	**48.5**	**Top ten total**	**6,241,000**	**87.0**

For example, the port of Los Angeles/Long Beach is one of the busiest ports in the US and received over three million cargo containers in 2001; approximately half of the total traffic arriving at US ports. One such shipment at the Port of Oakland is shown in the figure below.

Fig 1.1 A loaded container ship at Port of Oakland

The rate of container arrivals at US ports is expected to increase dramatically over the coming decade. The West Coast ports of Los Angeles/Long Beach, Oakland, and Seattle are currently processing 11,000 containers per day, or 8 per minute on a 24/7 basis. With so many containers and a large volume and mass of cargo in each one it is clear that these containers provide an attractive venue for smuggling illicit material into the US, including weapons of mass destruction (WMD). Because successful delivery of just one such weapon can have catastrophic consequences it is essential that all cargo containers entering the US be screened with an extremely high probability of detecting any WMD hidden within. The cost of failure is very high. An OECD report[2] estimates that a successful WMD attack would shutdown the entire maritime shipping system for a period up to 10 days and this would produce economic costs in the US alone of up to 58 billion dollars.

The number of cargo containers is sufficiently large that the time available to do an inspection would have to be short, about one minute. Inspecting the millions of cargo containers that enter the US by truck, rail, ship or aircraft is a daunting task. The seriousness and difficulty of the problem has been summarized a number of places including a recent report[3] of the CISAC at Stanford, a PNL report[4], a GAO report[1], and elsewhere[5-7]. Quoting from the President's announcement of the homeland security program: "The Department of Homeland Security would make defeating this threat a top priority of its research and development efforts. This nuclear denial program would develop and deploy new technologies and systems for safeguarding nuclear material stockpiles and for detecting the movement of those materials. In particular, it would focus on better detection of illicit nuclear material transport on the open seas, at U.S. ports of entry, and throughout the national transportation system."

Chemical weapons (CW) that are potentially present in cargo may or may not have distinctive chemical vapors allowing their detection, but they have no

radiation signatures that facilitate passive detection by nuclear means. Among nuclear weapons the ^{239}Pu components have weak but sometimes detectable radioactive emissions and they may be detectable using passive nuclear techniques, though detection is not reliable. On the other hand, ^{235}U in the form of "highly enriched uranium" (HEU) components have only weak, low-energy γ-ray emissions[8], with principal emission at 185 keV, that are severely attenuated by even small cargo over-burden so that they are nearly impossible to detect using passive nuclear techniques. This problem is even more difficult because natural radioactive decay of ^{235}U produces negligible neutron emission (~0.006 n/s per kg)[9]. For these reasons the concept described below utilizes active neutron interrogation to stimulate neutron capture γ-rays for the identification of chemical weapons and to produce detectable delayed fission product neutron and γ-ray emission for the identification of fissionable material. Unfortunately, none of these techniques are capable of identifying biological weapons.

Work reported in the following sections will focus on detection of shielded HEU and should apply to the detection of Pu. The technique described here utilizes large, high-efficiency detectors that will also be useful in passively scanning cargo containers and may detect ^{239}Pu by its normal radioactive decay. Some initial work was done here in the detection of explosive (HE) and chemical weapons (CW) using neutron-capture or neutron inelastic scattering γ-ray emission to provide remote chemical assay of unshielded targets, however it is not the focus of this paper. While Pu, HE, and CW detection may be within the capabilities to be described, the technical approach here will be optimized for the detection of shielded HEU.

1.2 Conventional neutron interrogation to detect SNM

Active interrogation methods are considered to be the only feasible option for the detection of HEU, because simple passive detection methods are made difficult by moderate amounts of shielding. The same methods of active interrogation can be used to detect plutonium. Intense fluxes of γ-rays or neutrons may penetrate cargo and/or shielding within which a mass of HEU is hidden and generate a characteristic signal that may be detected. There are at least four potentially viable approaches to detection of SNM and they are distinguished by the interrogation source (neutrons or γ-rays), and the induced radiation signature (neutrons or γ-rays). Passive radiation measurements and radiographs to locate high-density components buried within an otherwise low-density cargo may augment these four approaches.

Earlier work in detection of SNM focused on emission of delayed neutrons by fission products[10-13] following neutron-induced fission. Delayed neutrons are emitted from a fraction of a second to a few minutes after fission and have lower energies than the fast prompt fission neutrons. While delayed neutrons can be a reliable indication of SNM present, their yield is low [14], approximately 0.008 per fission in ^{239}Pu and 0.017 per fission in ^{235}U. More importantly, delayed neutrons are emitted at relatively low energy [15, 16] (200-500 keV) and are rapidly attenuated in low-Z hydrogenous cargo so that SNM is difficult to detect in the presence of cargo. The energy and die-away time distributions of delayed neutrons differ from the energy and time structure of natural radioactive backgrounds, thus providing a distinctive signature for Pu or

HEU. There are very few sources of delayed neutron emission other than fission products. This method has been demonstrated by VNIIA and RIPT (in collaboration with LLNL on an ISTC project) to measure HEU in luggage and at LANL to produce a package monitor. Russian work demonstrated the ability to detect 15 g of HEU in a 20 second measurement and detect the presence of a a small amount of shielding around the HEU by the anomaly in the neutron die-away. Further, in a second experiment, they produced a directed thermal neutron beam and were able to scan luggage, with a sensitivity of 2 g of ^{235}U in a 100-second measurement. However, all of this work was done with close access (10-20 cm) and without excessive shielding around the uranium. Results indicate that detection performance is rapidly degraded by introduction of cargo or the access restrictions imposed by the cargo container.

Delayed neutrons are uncommon in the natural radioactive background and thus generally provide a distinctive signature of fission products and thus of SNM presence. The exception to this is the case where 14 MeV neutrons are used for the interrogation. There is a reaction in oxygen, ^{17}O(n,p)^{17}N that produces delayed neutrons with a 4.2 sec half-life. The threshold for that reaction is high, 10.1 MeV, so softening the neutron spectrum can reduce or eliminate this interference with detection of SNM.

1.3 Other active methods to detect SNM

Utilizing γ-ray radiography the object is typically irradiated by an isotopic source of ^{137}Cs or ^{60}Co. Transmitted γ-rays can be detected in a detector array to provide a density image. A density image can offer another means to "see" inside a cargo container. This method has been implemented by SAIC[17-20], San Diego to radiograph the contents of cargo containers.

Some radiography systems utilizing accelerator sources have been extended to energies high enough ($E_\gamma > 5.6$ MeV) to produce fission in SNM and provide a new capability for γ-ray interrogation. At the same time neutrons from (γ,n) reactions may be detected due to high Z materials. This technique is utilized by INEEL and ARACOR[10, 11, 21]. The commonly occurring low and mid-Z elements typically have photo neutron emission thresholds above 6-7 MeV, while high-Z elements have thresholds below 6–7 MeV. It is not known at this time how accurately Z can be determined using the threshold effect. However uranium may stand out in such a measurement, since the nearest high-Z elements in common use are Pb (Z=82) and Bi (Z=83). In addition to this signature, the delayed neutron signature from (γ, fission) reactions may be detectable, because cross sections for photo neutron emission and photo fission are roughly comparable for ^{235}U in the energy range of interest. Some work in this area has been done by James Jones at INEEL[10, 11, 21], using a tabletop electron Linac (4-11 MeV) and by LANL using a 6, 8 and 11 MeV Linac[22, 23]. While the method can penetrate cargo containers and detect fissile materials, a disadvantage of this approach is the inability to detect hazardous contraband and explosives signatures simultaneously.

1.4 A new signature: Delayed high-energy γ-rays

There are many short-lived fission products that produce abundant γ-rays following β-decay and many have half-lives are in the range 1-60 sec. Some of

the β–decays have very high energies allowing population of highly excited states and copious emission of high-energy γ-rays that are distinct from the natural background radiation where high-energy γ-rays are almost nonexistent. Utilization of this signature for detection of SNM was first proposed recently by Norman and Prussin[24] and it is the primary tool used here to detect well shielded SNM. Details of this signature will be discussed in a later section. The advantages are:

- Delayed high-energy ($E_\gamma > 3$ MeV) fission product γ-rays are produced with total intensities approximately ~ 10 times larger than that of delayed neutrons in thermal neutron fission of ^{235}U or ^{239}Pu.
- High-energy γ-rays suffer 10X-100X less attenuation in thick cargos than is the case for delayed neutrons.
- High-energy γ-rays are a distinctive signature of SNM. They are generally not present in the normal radioactive background and not produced in high abundance by neutron activation of cargos or cargo environments.

This signature has not been utilized in earlier reports of neutron or γ-ray interrogation of cargo. The detector technology for harvesting the substantially larger flux of γ-rays escaping a thick cargo is well developed and costs are reasonable. The details of possible interferences from background and other sources from a broad range of cargo types have not been developed and are the focus of the work reported below and to be done in the future.

1.5 Detection of Chemical weapons and explosives

Considerable work has been done by others to develop neutron interrogation technology for detection of unshielded HE. Some of the systems providing remote chemical assay for HE detection are expected to provide similar capability for CW detection. Identification of the combinations of these elements in a sample is adequate not only to distinguish the CW materials from HE, but also to distinguish the CW agents from one another. Interrogation systems developed over the last three decades rely on characteristic neutron-capture or inelastic neutron scattering γ-rays for identification. The method has been applied to chemical weapons and explosives in munitions by LLNL[25] and AWRE, finding hazardous materials in luggage by VNIIA, using a 14 MeV neutron generator. A similar approach is used at INEEL, using a ^{252}Cf source. Thermal neutron capture γ-ray based chemical assay has been used as well[26]. Pulsed generators can provide elemental assay for drug and HE detection OSI (formerly Ancore and SAIC), and by Pulsed Fast/Thermal Neutron Analysis, PFTNA[26-34]. Similarly, fast neutrons have been used in systems such as NELIS[27] and PELAN[35-37] for explosives in munitions and utilize time-of-flight to delineate depth in the cargo and neutron capture γ-rays to provide remote chemical assay[28-30, 32, 33, 38-40] or even imaging of certain elements[39, 41]. These technologies have been reviewed by Martz & Griffin[42], Kahn[43] and some of the technical challenges are summarized by Micklich[40] and Moss[23]. Those techniques developed earlier may be applied here to augment the capabilities of this system. But they will not be discussed in detail because our main focus is the detection of SNM.

2 Neutron interrogation concept

2.1 Relationship to other components of container security

The basic interrogation concept is illustrated in the flow chart below.

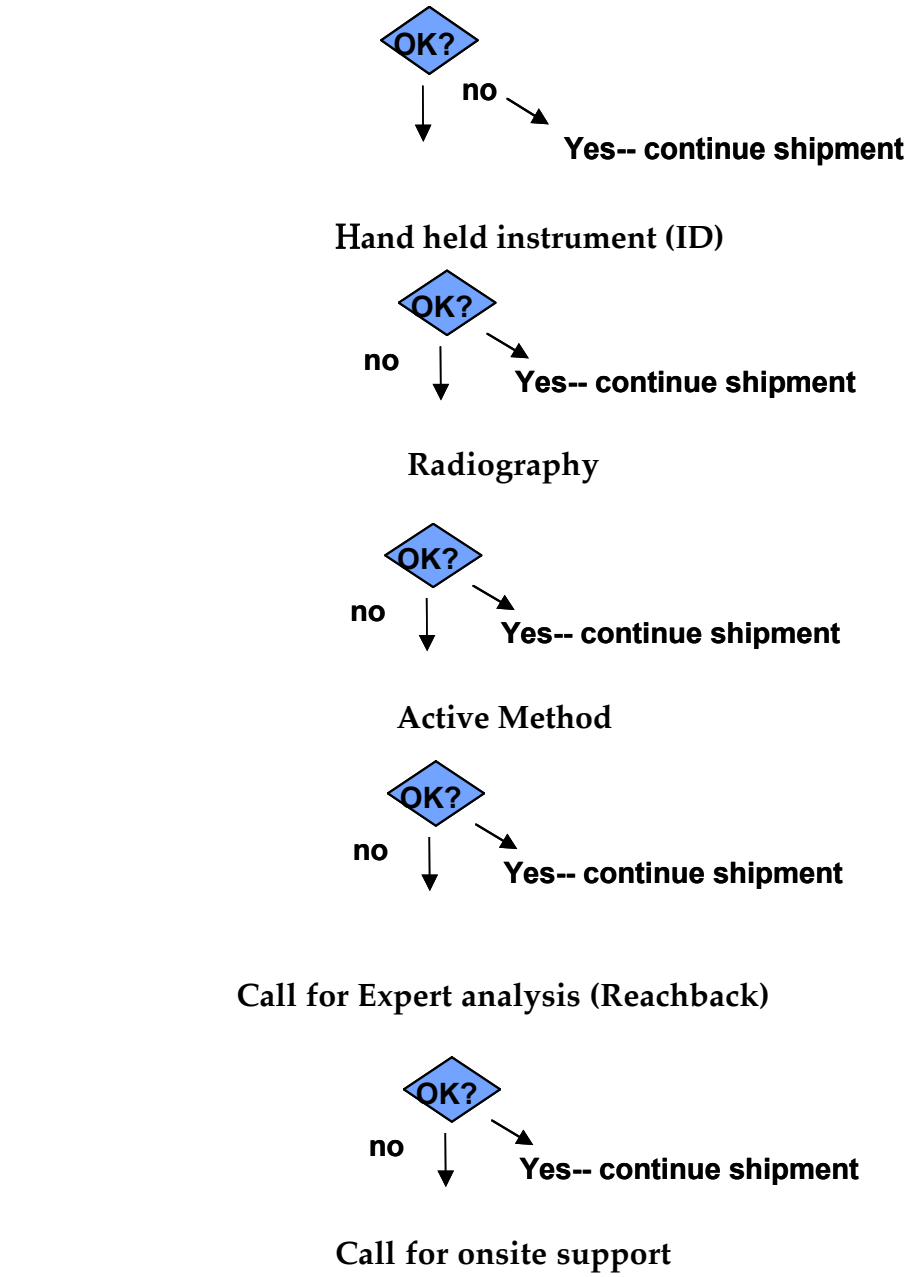

Figure 2.1.1 Architecture of a cargo inspection system

Currently radioactive items are noticed by an initial readout on a passive instrument, such as a radiation pager or portal monitor. Where present, handheld instruments are used to verify the signature and determine if the radiation is naturally occurring or medical. At this point, a container may be radiographed to look for discontinuities. If a discontinuity is found, the cargo container is unpacked by hand, taking several hours. In the above flow chart, we added neutron interrogation when passive measurements and radiography show a positive result. Alternatively, the neutron interrogation step could go in conjunction with the radiography step, since they are not mutually exclusive. The neutron interrogation step would identify the presence of fissile materials or other WMD contraband. The method could be used at a port of origin or a port of entry.

2.2 Goal of the neutron interrogation system

The goals of the interrogation system are:

- Reliably detect 5 kg HEU (≤ 1% error rates)
- Reliably detect 1 kg ^{239}Pu (≤ 1% error rates)
- Maintain reliability in cargos ranging from 0-60 g/cm^2
- Maintain reliability for a wide range of cargo types, including agricultural products, electronics products, and machinery.
- Maintain reliability even when time available for scanning is limited to about one minute.
- To the extent possible it should also detect CW or HE in amounts larger than 50 kg without compromising the ability to detect SNM

3 Laboratory Design

3.1 Simulations drive the design

We used detailed Monte Carlo simulations of radiation transport to and out of cargo containers undergoing neutron interrogation and signature detection to discern the presence of WMD materials. One goal is to learn by modeling experiments, how to make the models more realistic. We developed a complete model of a cargo container, source igloo, shielding walls, and the experimental facility in Building 231. We used COG8.43 [63] and the ENDL90 cross section library for all simulations pertaining to the dose estimation study. The final shielding design is shown in Figure 3.1.1.

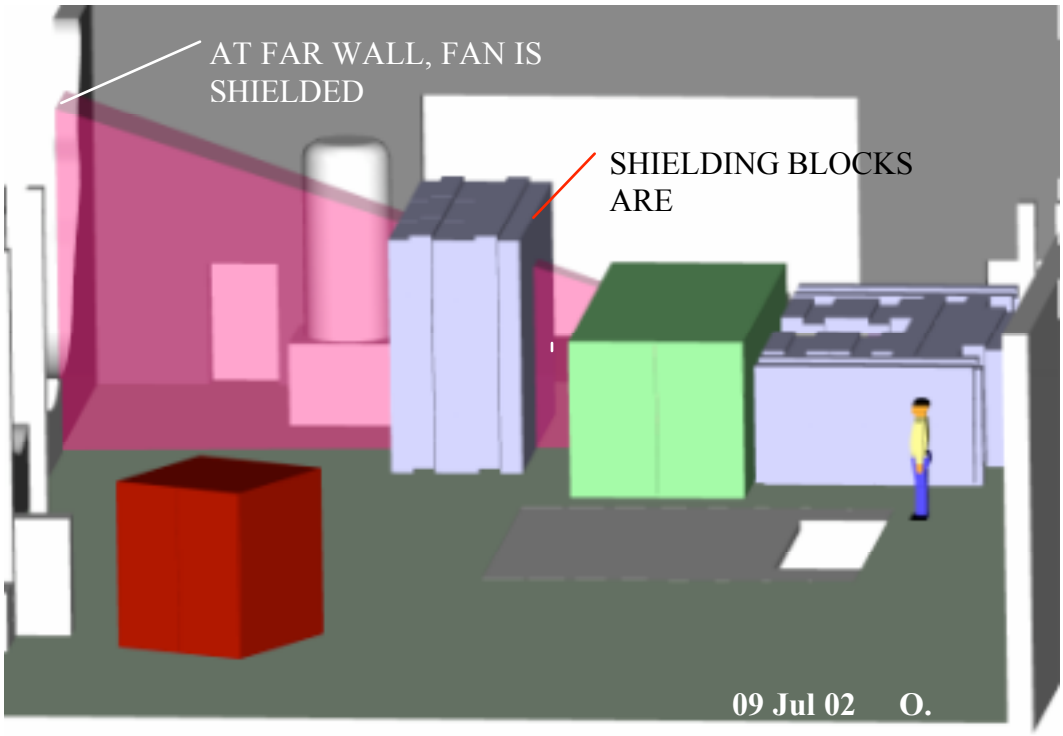

Figure 3.1.1 Graphic depiction of a modeling simulation of our active interrogation technique for detecting a hidden weapon of mass destruction. The maroon color depicts the neutron beam passing through a cargo container.

The shielding design was carefully planned to maintain doses as low as reasonably acceptable, ALARA, for workers both in adjoining offices and for the experimental team while making measurements. In this modeling, we performed radiation dose estimates using modeling simulations shown in Figure 3.1.2. In this dose model, we used accurate building dimensions and a 3D geometry. This was only possible with the use of ASCI computers; more than 1000 cpu hours were required for convergence. There was no accounting for holes in walls for plumbing and conduit penetrations that could provide line of sight. We used an average density/ average composition model for shielding components. The container was a simplified steel shell. These simplifications make the absolute dose somewhat uncertain, but the relative levels should be reliable in the vicinity of the experiment. We used dose phantoms in various places for person-equivalent doses. These were later validated by experiments using neutron output up to 2×10^{10} n/sec. We used these experiments to determine correction factors for calibrating our neutron monitors. These experimental measurements are shown graphically in Figure 3.1.3. Note that the highest doses occur only for the dose detectors placed on top of the structure near the source, a place where personnel will not be allowed. Table 3.1 shows excellent agreement between the predictions and measurements for the four occupied second-floor offices, outside the roll-up door and the operator's location. The measurements were made with a 9-inch NRD sphere attached to an E-600 ratemeter, "Remball" and the LLNL Remmeter, a lab-built Anderson-Braun Remmeter.

Table 3.1 Comparison of predictions with measurements of dose rates[1]

Location	COG prediction (mrem/hr)	Remball measurement (mrem/hr)
Operator	10.6	6.2
Outside rollup door	11.9	24.0
Office	0.8	0.3

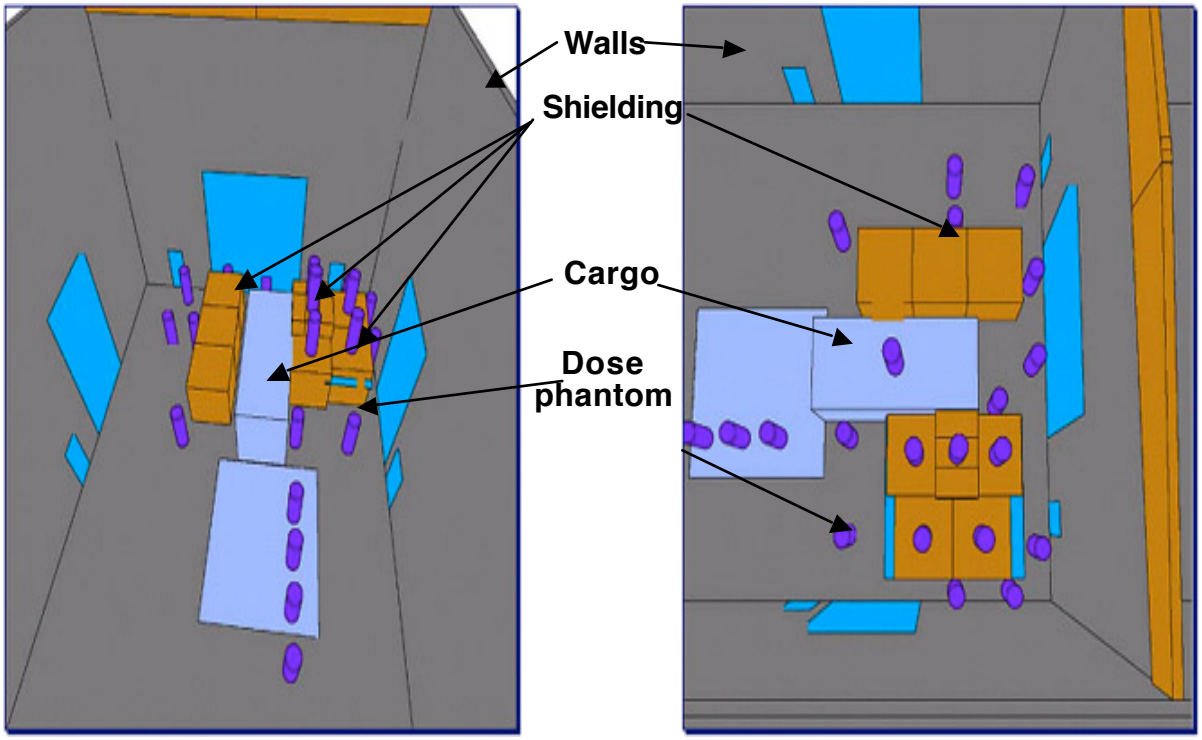

Figure 3.1.2 Diagram of modeling simulations. Doses were calculated for phantoms where indicated.

Table 3.2 shows the beam prediction vs. measured dose rates at the target location in the center of the container.

[1] All dose rates are for neutron doses only, photon doses add another ~10%. The maximum output was ~1E+10 n/s, 14 MeV energy, measured at the target location ~94" from the generator.

Table 3.2 Comparison of qualify factor for predictions vs. experiments. All data are in rem/hour.[2]

Quality Factor calculated	COG prediction	Remball	CR-39 foil
2.9	*1.7*	*2.9*	*3.6*

We spent some time understanding the proper instruments to use to measure dose rates for these experiments. Conventional remmeters are most useful for thermal neutrons, not pulsed neutrons from neutron generators. Measurements of the scattered neutrons were made using a 9" sphere remmeter and with 3" Cd-covered sphere to obtain the 9/3" sphere ratio. The procedure had been used in the past to determine the calibration factor to be applied to personnel albedo neutron dosimeters. The ratio of these spheres gives a rough estimate of the neutron energies. This ratio is large when high-energy neutrons are being measured and is low for highly moderated or scattered neutrons. These results will be compared to measurements made in our calibration facility located in Bldg. 255 [56].

We wanted to determine if the ^{6}Li borate TLD in the personnel dosimeter will flag the neutron exposures. The CR-39 foils in the personnel dosimeters are not evaluated unless the ^{6} Li borate TLD in the badge indicates 15 mrem of fast neutron exposure has been received. This "flag" is obtained from the thermal neutrons in the area. Measurements of the thermal neutron dose rates around the accelerator were made using the bare and cadmium covered probe from the 9-inch sphere remmeter. These data will be compared to the data obtained in our calibration facility in Bldg. 255. This will assure that the CR-39 foils will be evaluated if significant fast neutron exposure has occurred and that an appropriate calibration factor is applied.

Additional survey instrument measurements of the dose rates were made using the "Slab" neutron instrument, the 9-inch sphere remmeter and the SWENDI-II Wide-Energy Neutron Detector [57, 59]. The slab instrument is very sensitive and we were able to detect neutrons at the South end of the hallway of Bldg. 231. The neutron dose rate at the end of the hallway is negligible, but detectable. There is good agreement between the readings of the three instruments. If there were an abundance of 14 MeV neutrons, the reading of the Swendy would have been higher than the other instruments. The fact that it was not, indicates that there are few high-energy neutrons present. There is however, a large disagreement between the relative neutron dose rate measurement obtained earlier with the accelerator operating at 2×10^{10} n/sec, and the measurements made recently with the accelerator operating at 1×10^{9} n/sec. This difference needs to be resolved.

We have obtained Bubble neutron dosimeters to be used in this study. The Bubble detectors have an almost flat energy dependence for neutrons with energies from about 300 keV to 14 MeV. We intend to compare the bubble chambers readings to those of the neutron instruments and to the CR-39 dosimeters. The neutron instruments are known to under respond to 14 MeV energy neutrons. The CR-39 has an energy dependence that is low at 14 MeV by

[2] Beam measurements were corrected by Hankins' energy correction factors of 1.5 for the Remball and 2.5 for the CR-39.

42% when compared to a bare Cf^{252} neutron source. If the instruments and the CR-39 dosimeter do not have the same dose reading as the Bubble detectors, then we will need to determine what neutron spectrum could cause the disagreement.

The design of the shielding and experimental layout had to take many factors into account. There were adjoining offices and labs, so the neutron beam was tightly collimated to achieve ALARA. We were further restricted by floor loading limits, a pit (shown as the light blue rectangle at the bottom of the left-hand drawing in Figure 3.1.2), several large machines which could not be moved, a roll-up door, and exits that must be maintained. We also wanted access to the cargo container so we could quickly change cargo-loadings and configurations. We refurbished and installed a high yield neutron generator that had size constraints as well. The shielding wall as built, is shown in Figure 3.1.4.

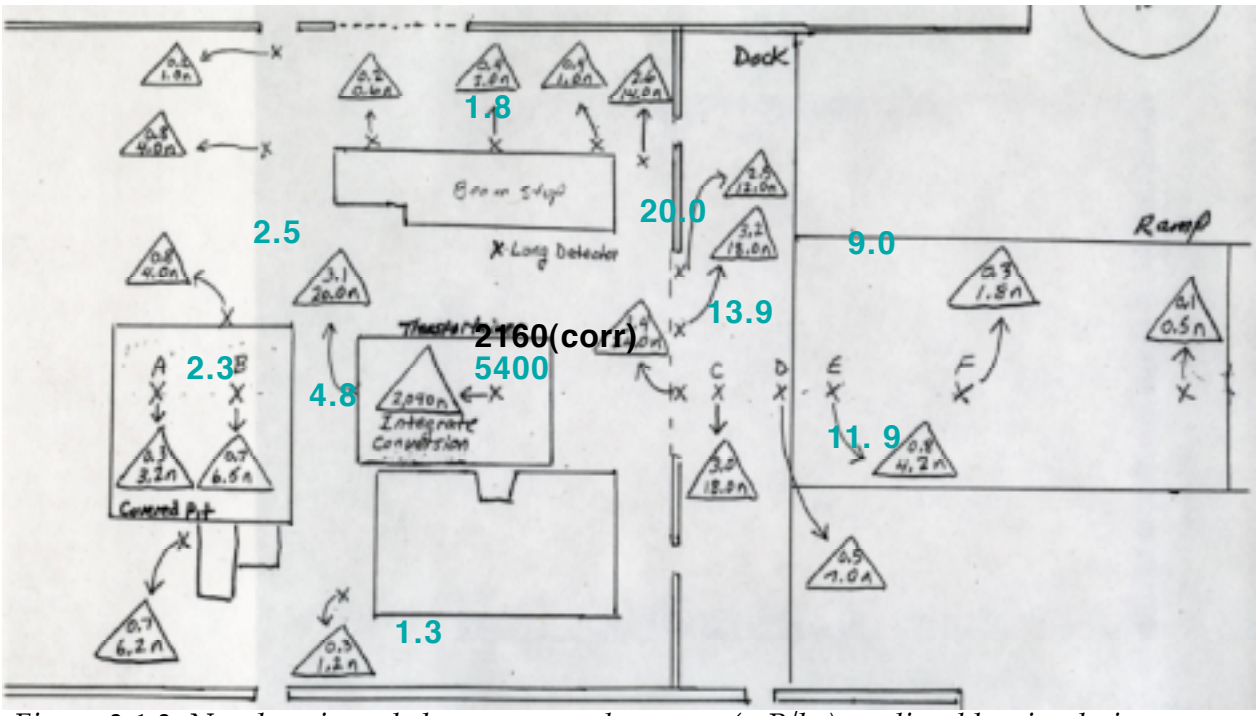

Figure 3.1.3. Numbers in teal show neutron dose rates (mR/hr) predicted by simulation and scaled to measured yield. Black numbers in triangles show gn dose rates (mR/hr) actually measured.

Figure 3.14. Shielding of the neutron source used cement blocks. The hole in the center is where the neutron source exits. A 20′ cargo container is placed in front of the cement.

We also collimated the source in a fan-shaped configuration to attempt to shield regions of neutrons which would only add to the background and not contribute to the interrogation of the item of interest. A drawing of this collimator is shown in Figure 3.15.

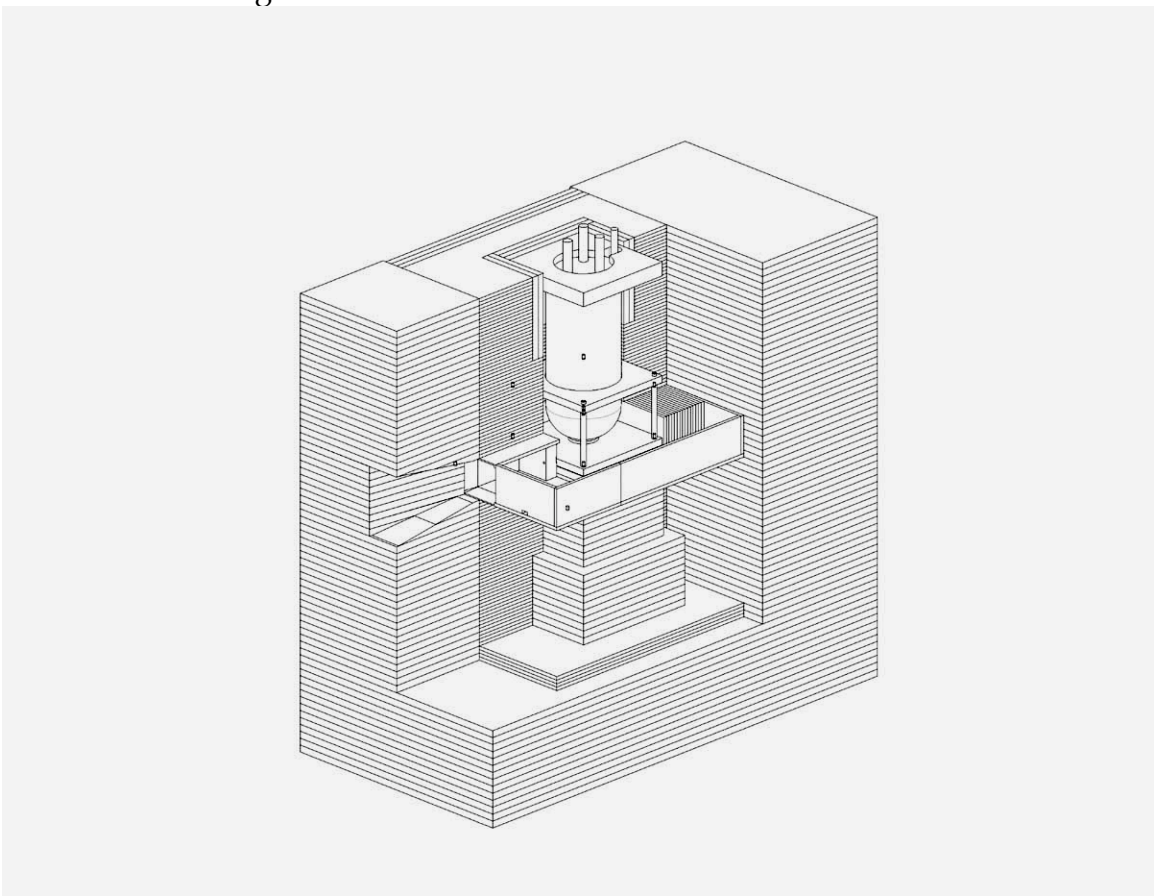

Figure 3.15. Mechanical drawing of fan-collimator. Neutron tube is seen in the center.

While the detector and source collimation minimized personnel dose, effects from background, energy and distance require further study and refinement.

Facilities were established for off-line analysis of data and re-running data in different configurations off-line. We used a web-site for sharing results. An electronic log-book with digital pictures of experimental configurations will be linked to each data-file. Modeling results for experimental configurations will be posted for comparison and summary.

3.2 Measuring the neutron yield of the accelerator

We reviewed several methods to determine the neutron yield of the accelerator, depending upon neutron energy. Sulfur pellets are activated by neutrons having energies above 3 MeV. We purchased 2-in Sulfur pellets and made a preliminary exposure to determine the relative activation compared to the smaller pellets used in the personnel criticality accident dosimeter [58]. A second exposure is needed to confirm the accuracy of the first test.

Aluminum is activated by neutrons having energies above 6 MeV. We did one preliminary exposure with several layers of Aluminum foils and determined we could detect the activation. We have obtained high quality Aluminum disks, 1-inch diameter x 1/8in thick, for use in future exposures.

Niobium is activated by neutrons having energies above 9.5 MeV We ordered some Niobium foils and will count them in follow-on work. Niobium is the best choice for determining the neutron yield of the accelerator since it is only sensitive to neutrons having energies of ~14 MeV.

Indium is activated by thermal neutrons and by neutrons with energies above 100 keV. We have exposed some indium foils at the accelerator both bare and inside B-10 loaded plastic. The Indium foil located inside the B-10 shield is used for the higher energy neutrons and the bare foil for thermal neutrons. The bare foil had a high activity but the foil inside the B-10 had only a small activation. Future exposures will require that thicker foils or several of the existing foils be used in the B-10 loaded plastic shields.

4 Cargo simulations

4.0 The role of modeling

Most of our efforts at exploring the effectiveness of various sources, detectors and data analysis have been experimental. However the wide range of possible combinations of cargo content and target arrangements make comprehensive experimentation impossible. Computational modeling offers a way to leverage the experimental foundation we've established. Our work relied primarily on 3-dimensional Monte Carlo simulation of the radiation flow from source to target and from target to detector. Our intent was to create a synergy with experiments that would allow iterative refinement of both the model and the measurements. Several simulation studies were undertaken during the course of this research. One of them, the dose estimation study, was described above. Others were undertaken to:

1. Find the optimal arrangement of cargo simulant that would minimize the time and effort of conducting experiments while providing realistic degrees of attenuation and moderation of source flux.
2. Predict the neutron and gamma fluences into the bounding surfaces of postulated HEU-bearing targets and candidate detectors.
3. Comprehensively model proposed active neutron experiments investigating use of delayed neutrons from fission reactions as signature for presence of highly enriched uranium (HEU).
4. Modeled feasibility of using large liquid scintillation detectors being added to the active neutron experiment. The results verified the adequacy of the baseline flux of particles (neutrons and gammas) into the detectors.

4.1 The basic model of container and cargo

In the initial stage of our modeling, we developed an adequate geometry of a common cargo container. We ignored corrugated walls and structural skeleton, but accurately accounted for average steel wall thickness, as well as wooden components that play a part in moderating the source neutrons. (Structural steel does increase neutron scattering but ignoring it will not alter the fundamental result.)

Determining the composition of typical cargo, and simulating it, were more challenging problems. We obtained cargo manifest data for west coast ports for the years 1999 and 2000, and used year 2000 totals from the Port of Oakland as a typical composition. We reasoned that the best basis for breaking down the set of possible cargoes was by their tendency to attenuate the candidate radiation signatures for disclosing embedded HEU. We therefore classified the common cargoes into categories by similar average atomic number and the likelihood of included voids. These categories are shown in the form of a pie chart in Figure 4.1.1.

Note the prevalence of hydrogenous products such as foodstuffs and wood products. We began our by modeling with these low-Z materials as simulated cargo, since we expect hydrogenous products to represent the greatest challenge to neutron interrogation. The first simulated produce model emulated potatoes and air, with average material densities consistent with the range of loads expected for typical containers. As seen in Figure 4.1.2, the relatively short mean free path for moderated neutrons in bulk of produce limits the flux into the object being interrogated. For comparison, the mean free path of a neutron in air is 20 meters. Next we developed a canonical low-Z cargo model based on plywood ($C_6H_{10}O_5$) hydrated to 12% water by weight. This closely approximated the plywood cargo simulant used in our Cargo Test Facility experiments, and was represented in the calculations using the measured density of 0.58 g/cm^3 as determined from the plywood in the experiments.

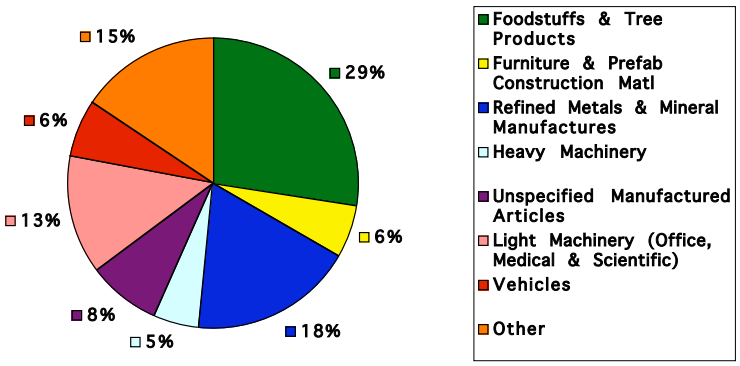

Figure 4.1.1 Fractions of major cargo categories by weight, passing through the Port of Oakland in the year 2000. The categories were chosen to exemplify distinct ranges of atomic number. Note the large fraction of hydrogenous foodstuffs and wood products.

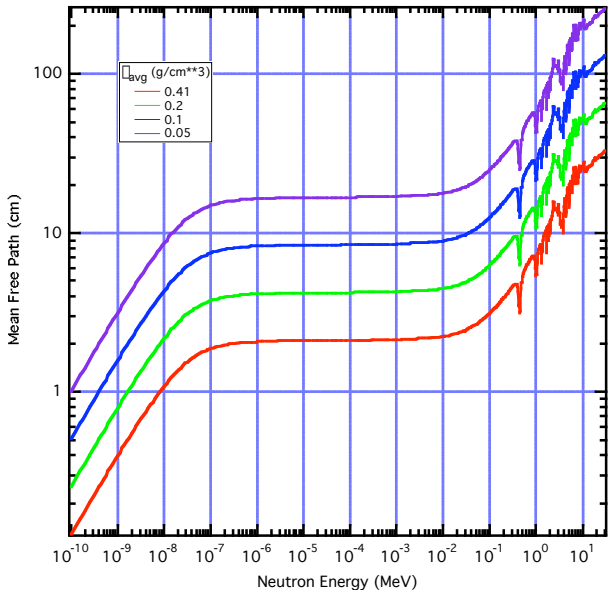

Figure 4.1.2 Neutron mean free path in simulated produce. The source of the data was ENDFB6.

For the canonical target, we used a 10 kilogram sphere of uranium-238. Our earliest calculations used no cargo simulant, but simply studied the distribution of fissions within the target. In this simple model, we predicted fissions for greater than 50% of incident neutrons that reach the target. The geometry of our more refined model is shown in Figure 4.1.3. Here the target was placed at the centroid of the container, between equal thickness layers of the simulated cargo.

Our container model used a simple steel shell with 2 mm steel walls and a wooden floor, based on measurements of the actual container. We assumed 14 MeV (d,t) line source in energy, line source in energy, emitting isotropically from a point in space. An idealized collimator was created through modeling an early collimator as designed and deriving an equivalent structure that would save simulation time by not following superfluous particle histories. The cargo density was varied from 0.1 – 0.4 g/cm^3 and consisted of vertical sheets of material in a reproducible arrangement. We used three types of cargo simulants. In addition to the low Z surrogate (plywood), we chose sheet aluminum and steel for the medium and high Z surrogates respectively. The detector was a 1-m^3 slab holding ^3He tubes in CH_2.For simple studies that gauged particle flux into its volume, the entire detector volume was modeled as an ideal absorber. Both of the Monte Carlo codes we used had the capability of recording the particle flow across the detector boundary in list fashion. This "virtual source" could then be used for subsequent studies of detector response.

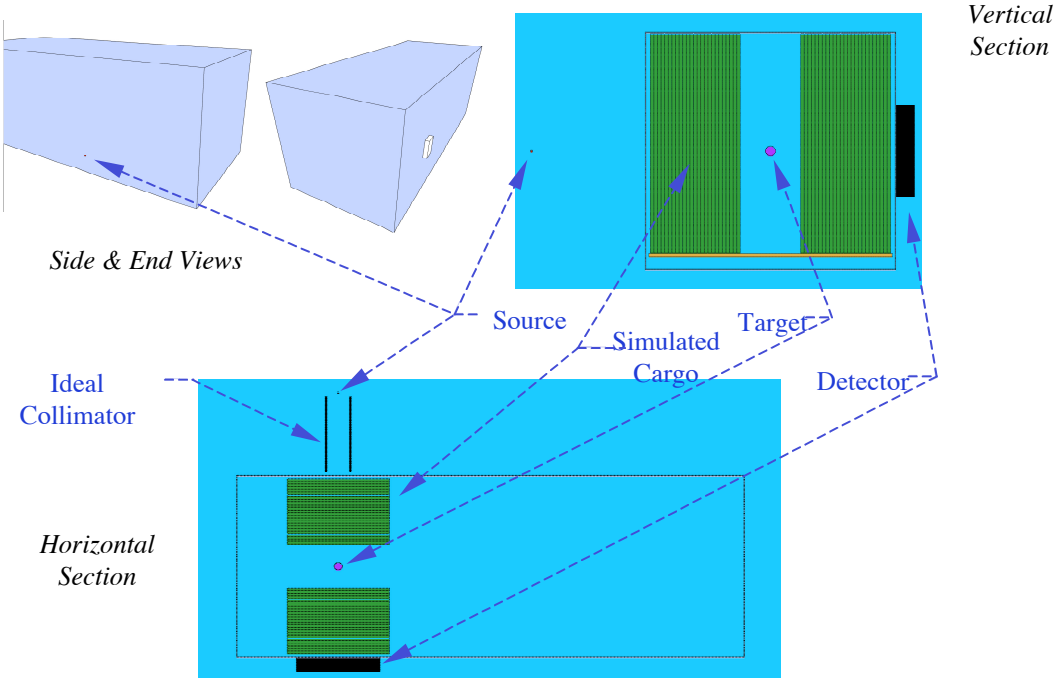

Figure 4.1.3. Cross sections of cargo container used for neutron simulations

The creation and detection of the fission signature is best viewed (and modeled) in stages. The first stage transports 14 MeV neutrons from the source to the target and records the fission rate and the number of neutrons emitted from it. Depending on the amount and composition of the cargo, the source neutrons may be underthermalized and not efficacious or over-thermalized and

never reach the target. Figure 4.1.4 shows the effect of cargo density on particle fluence. For comparison, we calculated both neutron and gamma fluence, integrating over both time and energy. As expected, at lower densities, neutrons are poorly thermalized and at high densities, the neutrons are strongly scattered by the hydrogenous material. Both detector and source need to be collimated to emphasize signal originating in the interrogating object. Time gating of signals may be desirable to record delayed emissions.

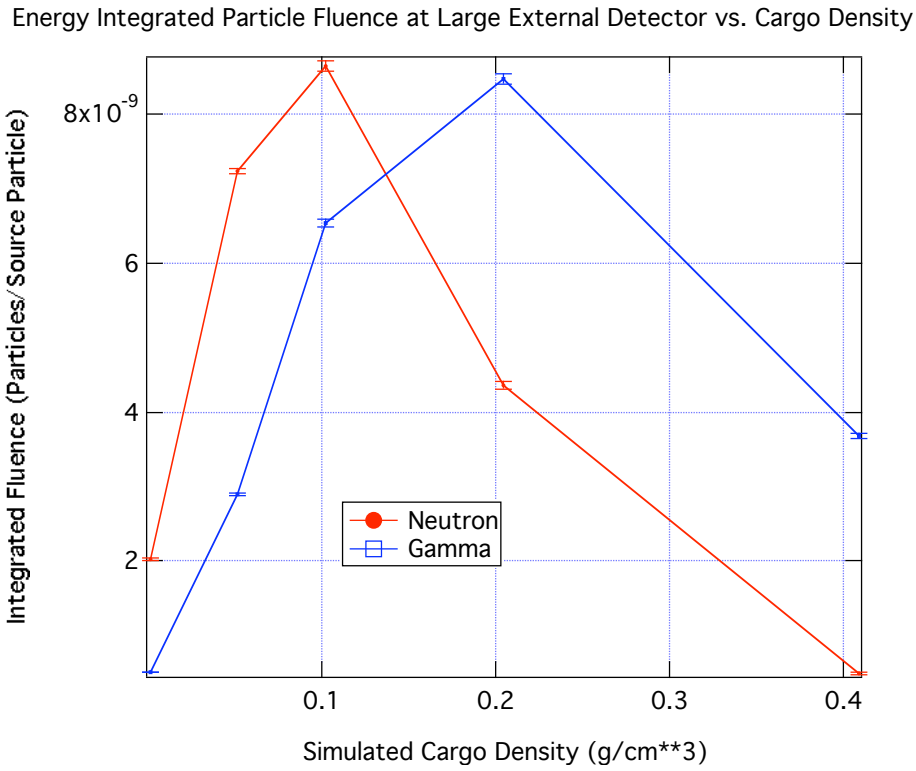

Figure 4.1.4 Plot of particle fluence integrated over time and energy versus cargo density for neutrons and gammas.

4.2 Cargo and composition parameter study

In our later calculations, we used the 14 MeV neutron source with a geometry that matched the design intended for the testbed experiments, including the fan collimation. The neutrons interrogated an HEU target in the form of a segmented sphere. The detectors were assumed to be large slabs of polyethylene with embedded helium-3 tubes. Both COG10.x [63] and MCNP4C2 [620 were used to examine two promising signatures: 1) gamma rays from inelastic neutron interactions with telltale elements in the target and 2) delayed neutrons from induced fissions in HEU.

In order to save calculation time, we broke the simulations down into stages:

1. Transport of source particles through the cargo stimulant to the bounding surface of the target.

2. Transport into the target inducing fission.
3. Transport of particles emitted from the target out to the bounding surface of the slab detector.
4. Transport into the detector volume leading to detection reactions.

Dividing the calculation in this way allowed us to cover a large number of parametric cases without the need to repeat portions of the simulation that were held constant. We used variance reduction techniques where possible to limit the number of particle histories needed to achieve satisfactory statistics. As expected, we found that signature strength depended strongly on the cargo amount and its composition. We found that source neutrons may be under-thermalized and not efficacious or over-thermalized and never reach the target.

We first compared time integrated fluxes by comparing calculated neutron and photon spectra for an 8 kg. HEU target. The comparison of the data, shown in Figures 4.2.1 and 4.2.2 show no distinctive indication of the presence of the ^{235}U. To improve discrimination, we decided to separate the prompt and delayed radiation coming from the target.

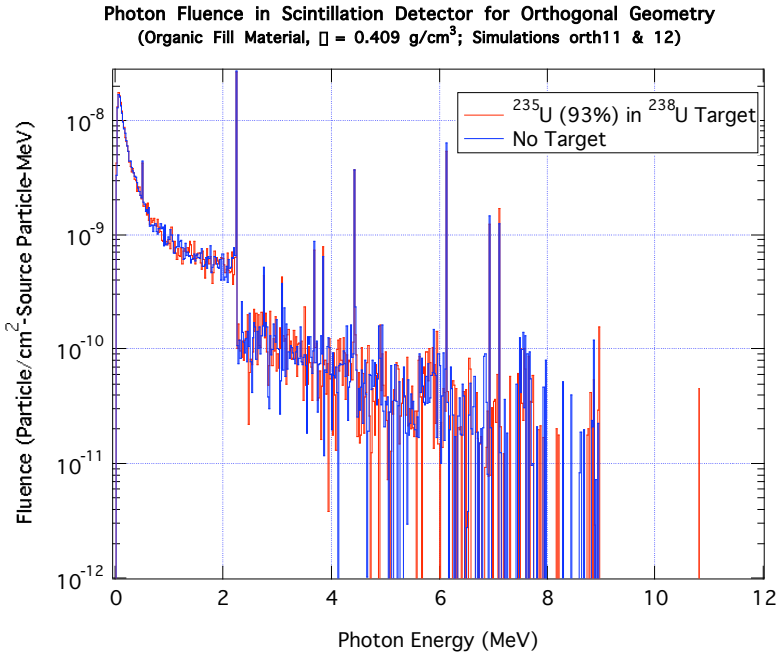

Figure 4.2.1 Photon fluence in scintillation detector. The cargo fill was organic with a density of 0.409 g/cm^3.

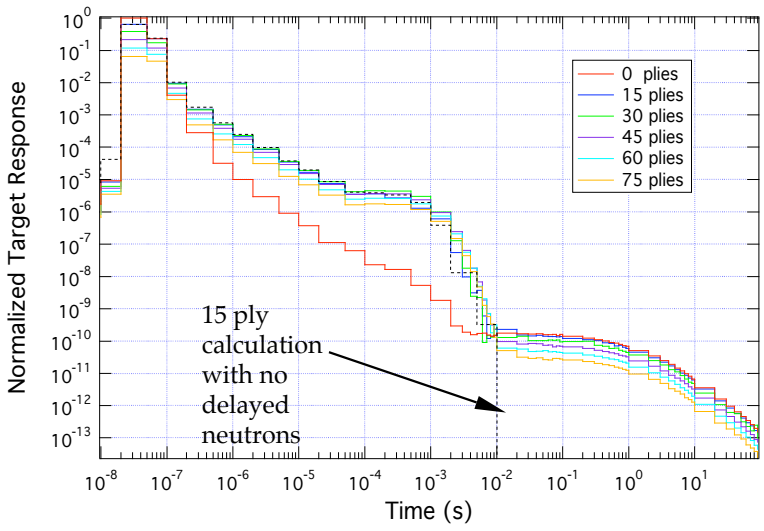

Figure 4.2.2 Neutron fluence into scintillation detector The cargo fill was organic with a density of 0.409 g/cm^3.

To distinguish the delayed neutrons we calculated the time evolution of the HEU target emissions in varying cargo load, seen in Figure 4.2.3. As seen in the figure, the prompt and delayed neutrons at the target are time-resolved and disparate in magnitude. The good news is that the resolution of prompt and delayed radiation appear to be independent of cargo load. However, the relative magnitudes of prompt and delayed radiation impose severe requirements on source contrast and detector efficiency, and may make practical measurements possible.

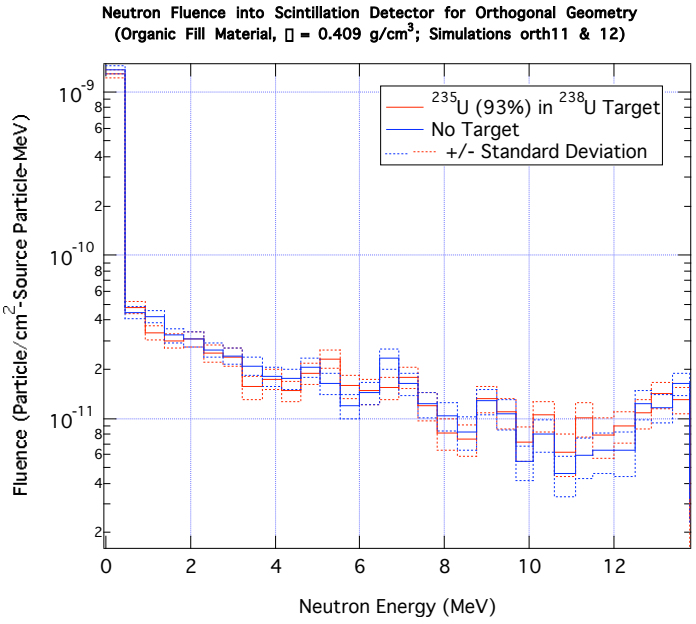

Figure 4.2.3 Time evolution of HEU target neutron response

The cargo loading affects neutron flux on the target and energy partition. In Figure 4.2.4 is shown the target response as a function of amount of cargo. The

mean free path of a neutron in wet plywood (12% by weight, density 0.58 g/cm^3) is between 6-10 cm and rapidly decreases with energy (Figure 4.2.5).

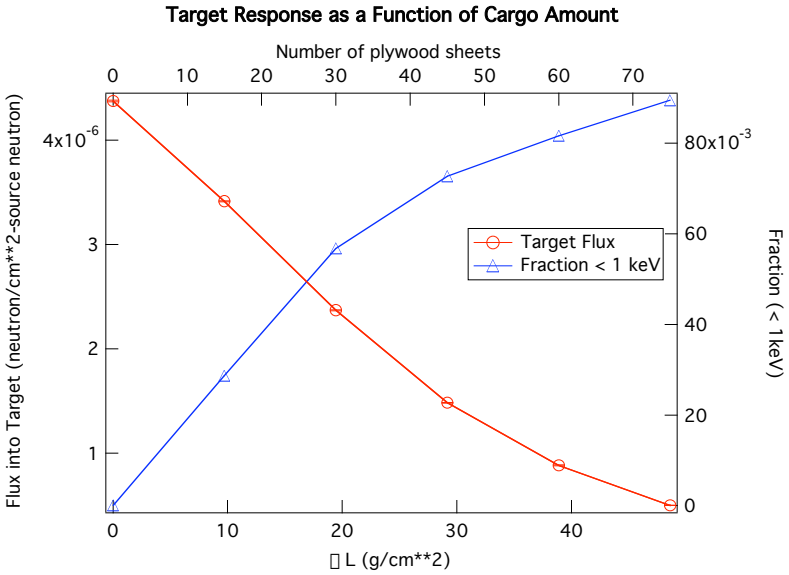

Figure 4.2.4 Target flux as a function of cargo loading.

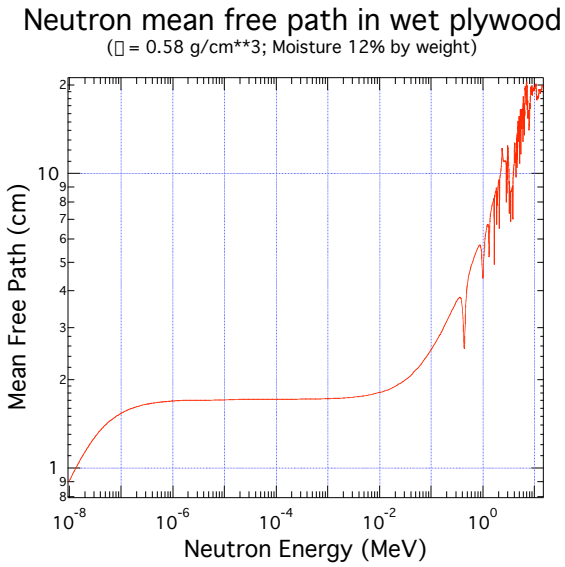

Figure 4.2.5. Neutron mean free path in wet plywood.

We then looked at the fraction of total target flux as a function of neutron energy, shown in Figure 4.2.6. When we calculated the flux for varying amounts of plywood, we found that the low-Z cargo simulant did not thermalize a significant portion of the source neutrons. Even the highest areal density shifts less than 1% of the population below 1 keV. Since the total neutron cross section of ^{235}U (Figure 4.11) varies strongly with neutron energy, a more thermalized

cargo or lower incident neutron energy would favor a higher detection efficiency of HEU.

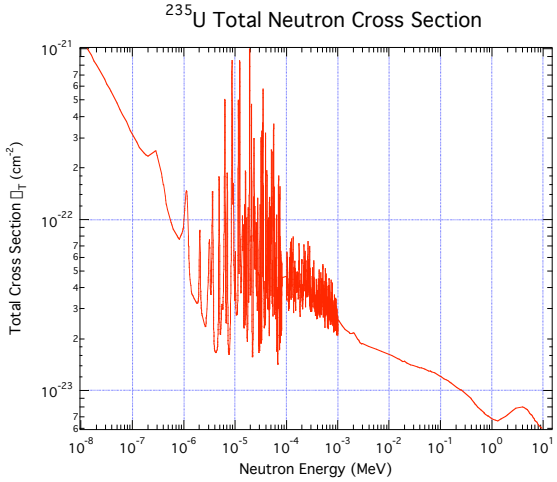

Figure 4.2.6 Fraction of total flux versus neutron energy.

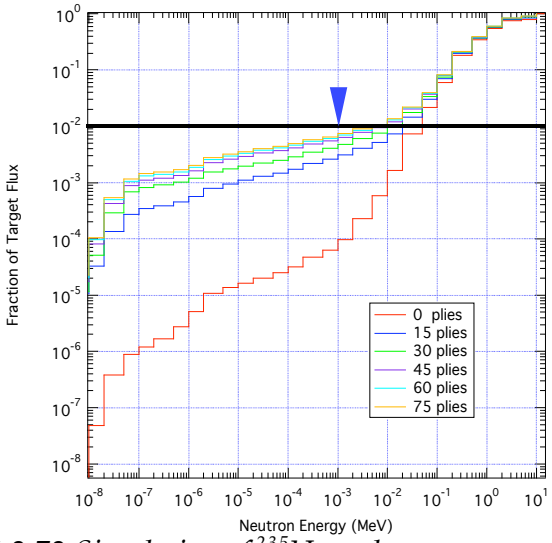

Figure 4.2.72 Simulation of ^{235}U total neutron cross section.

One challenge in the models is that the delayed neutron spectrum is "soft" and weakly penetrating, as seen by Figure 4.2.7 (reference). We calculated the flux into a 1m^3 detector, shown in Table 4.1. While the delayed neutron signature would also include the output of subsequent fissions produced in the target, only neutrons were accounted for in this suite of calculations.

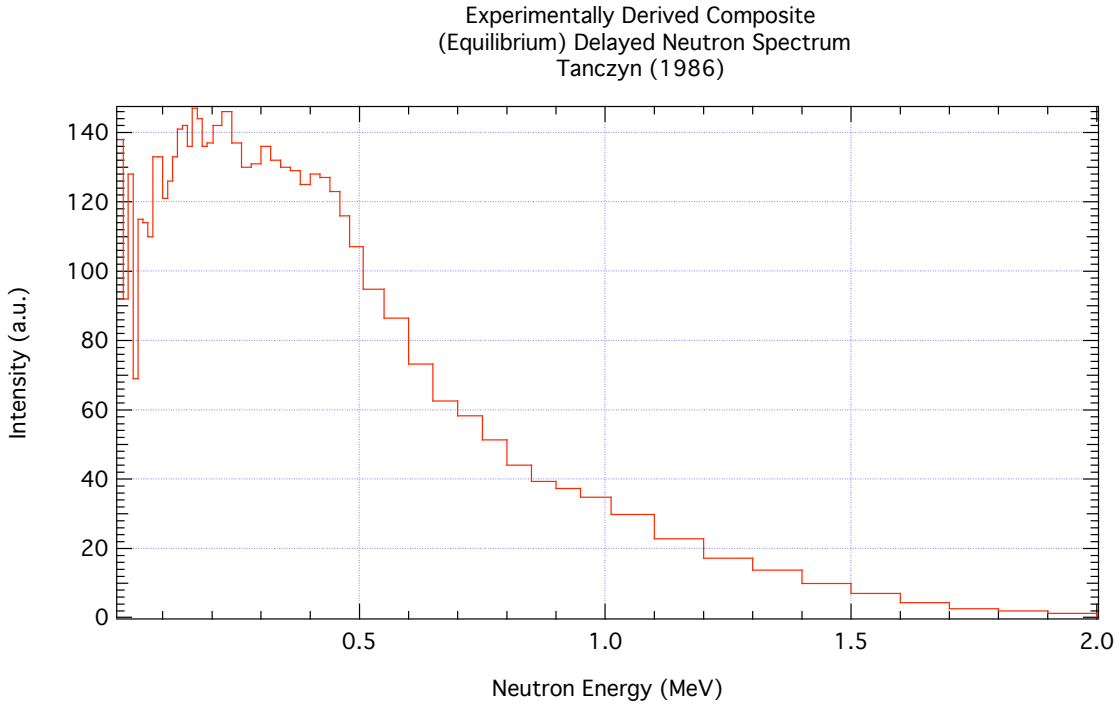

Figure 4.2.7 Experimentally determined delayed neutron spectrum from HEU.

Table 4.1 Delayed neutron signature with varying amounts of plywood.

□L (g/cm^2)	Number of plywood sheets	Neutrons/Source Neutron	+/-
0.00	0	1.0558E-07	5.8796E-10
9.723	15	7.7213E-8	5.8796E-10
19.45	30	2.8163E-08	8.8371E-10
29.17	45	1.1154E-08	1.0237E-09
38.89	60	4.0301E-09	7.0303E-10
48.62	75	9.6330E-10	1.7119E-10

We performed a study on the effects of cargo placement and size on the fission rate in the target. The results are shown in Figure 4.2.8. In the figure, the error estimates derive from one standard deviation of the total neutron flux through the target surface. The modeling calculations addressed the size, orientation and target offset of the cargo, as well as the presence of a symmetric load *behind* the target. The figure of merit was the fission rate per source neutron in the target. This is not a first order variation, i.e., alterations lead to 10-20% differences in the fission rate. The best arrangement (approximately 30% enhancement to the fission rate) would come from orienting the plies with their long dimension vertical and placing additional plies behind the target. The number of additional plies needed may be estimated by the value of the importance function for each "back" ply to the flux into the target. These calculated values converge more slowly than the detector fluxes and therefore

are approximate at best, but they seem to drop off rapidly after the first 15 plies in plywood, the first 5 in aluminum.

The effects on the fission rate are small (less than $\pm$ 20%) for these variations. The results indicate that the target could be scanned (translated) along the x axis for at least 6′ of the 8′ cargo length. They also suggest that placing cargo behind the target will recover some of the neutron flux – a more realistic scenario. The amount required is still to be determined. The most advantageous arrangement, particularly for the aluminum plate cargo simulant, would appear to be a vertical orientation of plies with some thickness of cargo added behind the target. The amount of backing required depends on the material type. No added benefit appears to come from having double size (8′high x 8′ wide) cargo sheets.

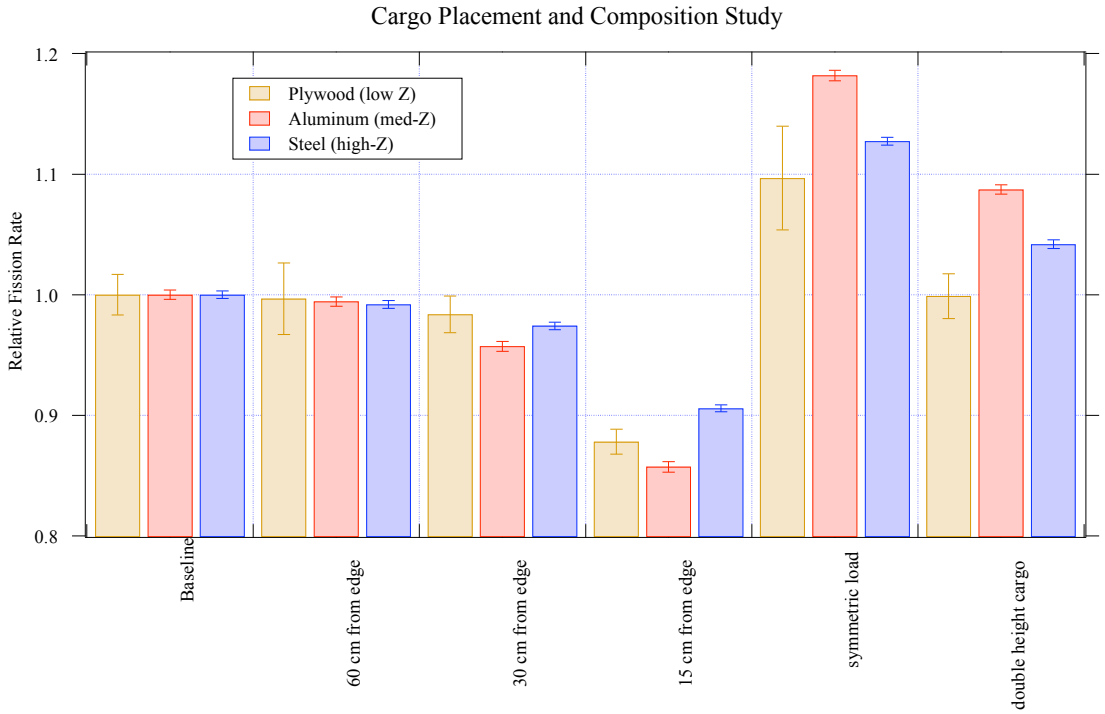

Figure 4.2.8 Cargo placement and composition study.

Further, we modeled the effect of load distribution in the cargo container for 1 kg of HEU. In this comparison, we modeled wood in 50.3 cm bundles. The arial density was 29.2 g/cm^2. We displaced the loads relative to the center of the container. In Figure 4.2.9, three geometries are shown, with the neutron source entering from the top of the diagram. Figure 4.2.10 is a bar chart of the results. The close-in loads (D=60, S=60) have a higher relative fission rate than loads where the HEU is further away from the shielding.

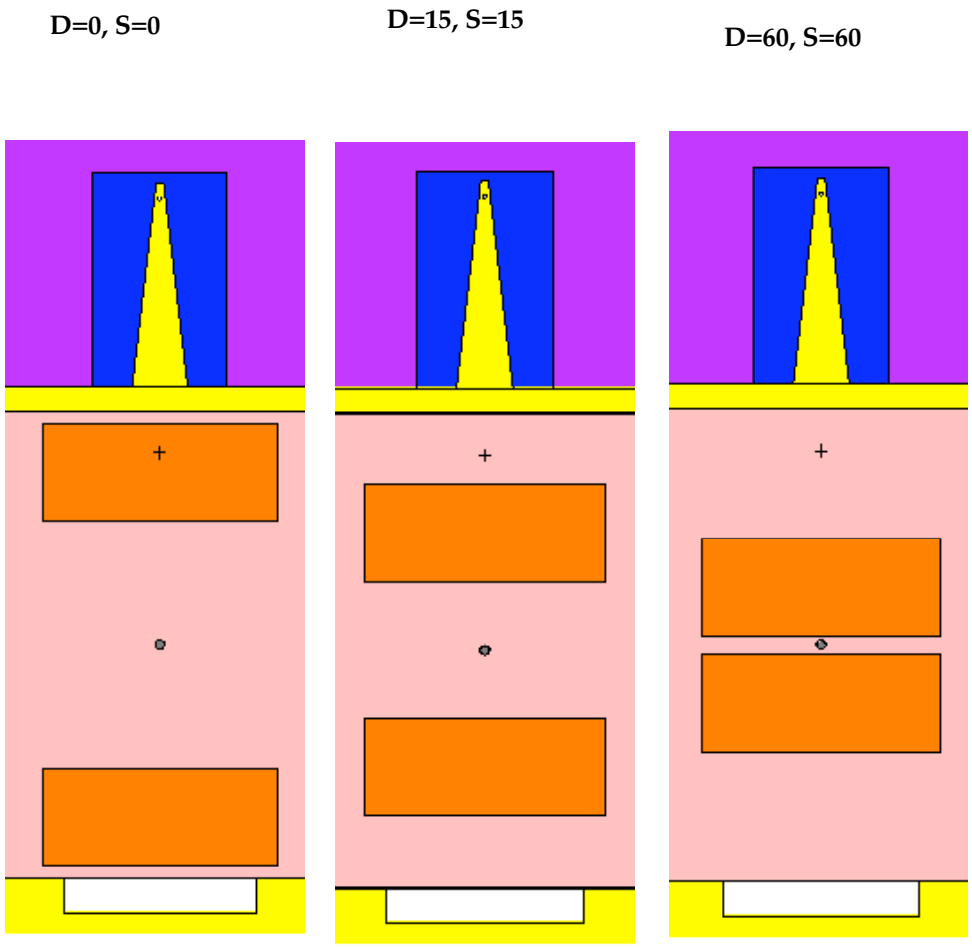

Figure 4.2.9 Geometry of load distribution study, as seen from above. The neutron source is emitted from a fan collimator, shown in the upper purple box. The cargo is shown in orange. The detector is in the bottom yellow box. D= detector-side, S-source side. The amount of displacement from the center of the cargo container is given in cm.

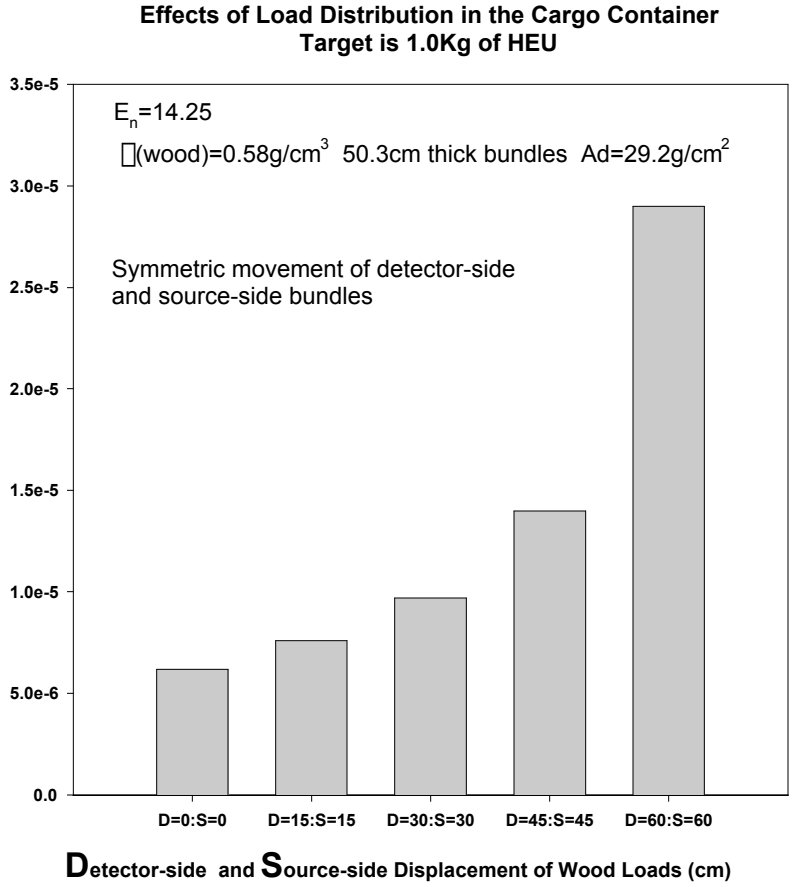

Figure 4.2.11 Bar chart of the load distribution effects. The ordinate is the fission rate. The geometry is shown in the previous figure.

We wanted to address the question of "How complete a representation of cargo entering the US do we achieve assuming homogenous materials with approximate atomic numbers?" Our studies, as described above, used three homogenous materials: plywood (low Z), aluminum (medium Z) and steel (high Z). Realistically, cargo shipments are heterogeneous, have complex shapes, and sample a broad range of the periodic table. We suspect that heterogeneous cargos will be advantageous to neutron induced approaches because of the varying densities will allow for channeling of neutrons to penetrate more easily into the cargo. Our test case used pallets of cases of wine arranged symmetrically between the source and the detector. We will consider both neutrons (delayed spectrum) and gammas (5 MeV) Failures to model "typical" cargoes using combinations should call the fundamental simplifying assumption into question. Figure 4.2.11 shows the geometry description of the model. We anticipate that we will be able to complete this calculation at a later date.

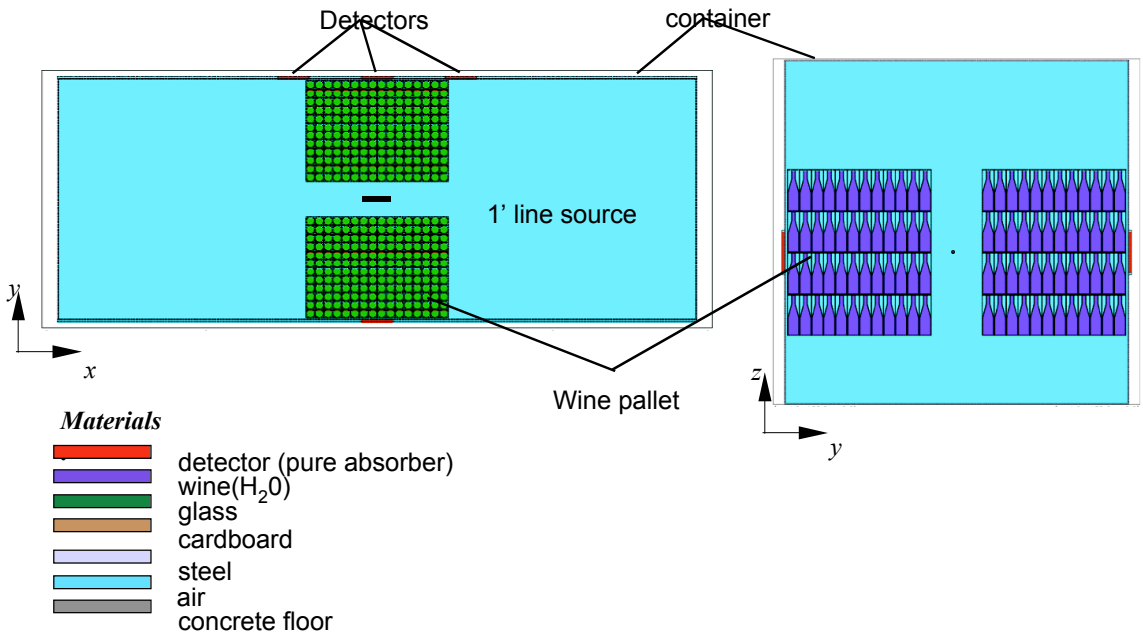

Figure 4.2.11 Heterogeneous cargo model: geometry description.

4.3 Challenges to modeling 'realistic' active neutron experiments

One persistent challenge in the simulations was the missing cross section tables in ENDFB6R7. We found many gaps in the data, such as argon, aluminum, germanium, sulfur, and others. These were evident in our initial studies where we tried to calculate simple activation experiments on HE and CW targets and many of the telltale gamma-ray lines were absent and important in understanding the gamma contributions to background and the high energy SNM gamma-ray signatures.

Variance reduction techniques for the most part didn't lend themselves to "compound" problems such as these. Our strategy was to divide up the problem into two or more stages.

5 High-energy □-ray signature of SNM

An alternative and untried approach is to detect SNM by its characteristic short-lived, high-energy fission product □-rays in between beam pulses. Prior to the recent suggestion of Norman and Prussin there is only one published effort[44] to look for fission products following photo-fission reactions where delayed fission product □-rays are utilized. A more detailed account is given in Slaughter, et al. [60].

Table 5.1.1 below summarizes the □-ray yields and compares them to the delayed neutron yield. Clearly, the □-ray intensity above 3 MeV is roughly a decade larger than the delayed neutron yield.

Table 5.1.1 Neutrons or γ-rays per fission

	^{235}U thermal fission	^{239}Pu thermal fission	^{238}U fast fission
Delayed neutrons[14]	0.015	0.0061	0.044
γ-rays[8] at $E_\gamma > 3$ MeV	0.127	0.065	0.11
γ-rays[8] at $E_\gamma > 4$ MeV	0.046	0.017	0.03

More importantly, high-energy γ-rays suffer much less attenuation in low-Z cargos typical of maritime container contents. The consequence is that high-energy γ-ray fluxes at the wall of the container are likely to be much larger than delayed neutron fluxes and thus potentially easier to detect.

The attenuation of delayed neutrons is more complicated to predict. The intensity of unscattered neutrons can be predicted to fall exponential according to the total neutron cross section. On the other hand many scattered neutrons will escape a cargo and can be detected, so the total cross section overestimates the attenuation of a useful signal.

We found that roughly ~ 10 times higher source intensity of the delayed high-energy γ-rays, but in addition the attenuation of these γ-rays may be up to 2-3 decades less than for the delayed neutrons in a thick (40–60 g/cm^2) cargo of agricultural products. The result is that the high-energy γ-ray signal leaving the thick cargo may be as much as 10^2-10^4 times larger than the delayed neutron flux.

6 Experimental validation of γ-ray signature

Some of the concepts presented in previous sections have been evaluated experimentally to assess their performance and illuminate technical difficulties. The technical challenges are substantially different for chemical assay to detect CW or HE than they are for detection of SNM. The former is based on analysis of neutron capture γ-rays with the beam on while the latter is based on analysis of high-energy delayed fission product γ-rays observed between beam pulses. Chemical assay is readily tractable for unshielded targets but is rapidly complicated by the presence of intervening cargo. Detection of SNM is based on a new signature introduced here for the first time and will be addressed in detail below.

6.1 Detecting the signatures of SNM

The new γ-ray signature was first determined in our collaboration with Norman and Prussin and they recently undertook experiments to verify its presence and intensity. The first of these experiments was carried out using a deuteron beam on a Be target at the LBNL 88″ cyclotron[24]. In those experiments the high yield predicted for these γ-rays was verified both for ^{235}U and ^{239}Pu, using very small samples, good detection geometry, and a well-

shielded analysis cell. Intense γ-radiation in the 2.5–6 MeV range was observed from small samples of HEU and Pu and there was negligible intensity when the SNM samples were removed and/or replaced by other materials such as iron, wood, or polyethylene. Decay curves were obtained there indicating that the high-energy γ-ray component decayed with a half-life of approximately 20 sec.

Subsequently, signature verification experiments have been conducted at LLNL using a collimated 14 MeV neutron source ($2x10^{10}$ n/s) irradiating a 22 kg target of natural uranium located within a standard 20 ft long cargo container. A picture of the lab with the shielded neutron generator on the right and cargo container in the center is shown below. Initially, a high purity germanium detector was placed on the cement blocks above and to the right of the cargo container. Since the detector was small, at this distance it was difficult to make signature measurements in a timely manner. In follow-on experiments, we placed the detectors much closer to the target and reconfigured the collimation to further optimize the measurements.

Figure 6.1.1 Cargo container lab at LLNL containing a collimated 14 MeV neutron source, a 20 ft cargo container.

The neutron source was located approximately 2.5 m from the target on the side of the cargo container (behind it in the figure) and produced a neutron flux of ~$2x10^4$ n/cm^2/sec at the target without shielding or intervening cargo. The target was a cylindrical container of metallic uranium beads making up a cylinder approximately 8 cm diameter by 15 cm long, at reduced density. A picture of it is shown below.

Figure 6.1.2 Natural uranium target used in foreground experiments. The ruler scale is in inches.

A typical setup is shown in the figure below.

Figure 6.1.5 Cargo is stacked into container between the source and target

The neutron generator was pulsed with a period of 60 seconds, operated at 50 % duty cycle, i.e. beam was on 30 sec and then -ray counting extended for 30 seconds between beam pulses. Due to the very small size of the HPGe -ray detector the count rates were low and data was obtained by accumulating pulse

height data over several hundred pulses. Following each pulse the data was acquired in 1-sec intervals up to 30 sec. At the end of a measurement the pulse height spectra corresponding to a single interval, cf. the interval 3-4 sec after beam-off, were summed together to produce a final set of 30 pulse height spectra. These measurements were repeated with the natural uranium present (foreground) and with the natural uranium replaced by an empty container (background), with the polyethylene beads still present.

Studies to determine the attenuation and thermalization effects due to cargo will be done as follow-on work. For these studies sheets of plywood, aluminum, or steel are stacked into the container between the beam and target, as well as behind the target.

7 Detector design

Rapid assessment of cargo container contents requires high signal-to-noise. Earlier sections showed that this signal is weak even with strong interrogation source strength. It is essential to have very high detector efficiency in order to detect the unique signals due to SNM fission product emission. As described in Section 5 there are far too many γ-ray lines among the 40 or so prominent fission products to be resolved even by a high-energy resolution spectrometer. A low-resolution detector will prove adequate for reliable detection of the SNM signature. In addition, the signature γ-rays are likely to scatter in thick cargos several times before escape. Consequently, although absorption is very weak and the total intensity is only moderately attenuated as γ-radiation transits the cargo, the photons are scattered in a way that decreases the intensity of the full energy peaks and increases the intensity of the underlying continuum spectrum due to Compton scattering in the cargo. Because of this high resolution spectroscopy is not useful or warranted. High efficiency, low-resolution γ-ray detectors are available, appropriate, and relatively inexpensive.

The concept studied here invokes 2-4 very large detector arrays sensitive to both neutrons and γ-rays, and able to distinguish the two radiation sources. They consist of a bank of liquid-scintillator-filled tubes spanning the full length and height of each container sidewall. These tubes are nominally 30 cm diameter by 3 m length and are aligned with their axis vertical. Two offset rows are emplaced to provide total coverage of each container sidewall. A total of 20 tubes are sufficient to cover one sidewall of the cargo container. A subset of 4 tubes has been assembled for evaluation and its schematic is shown below.

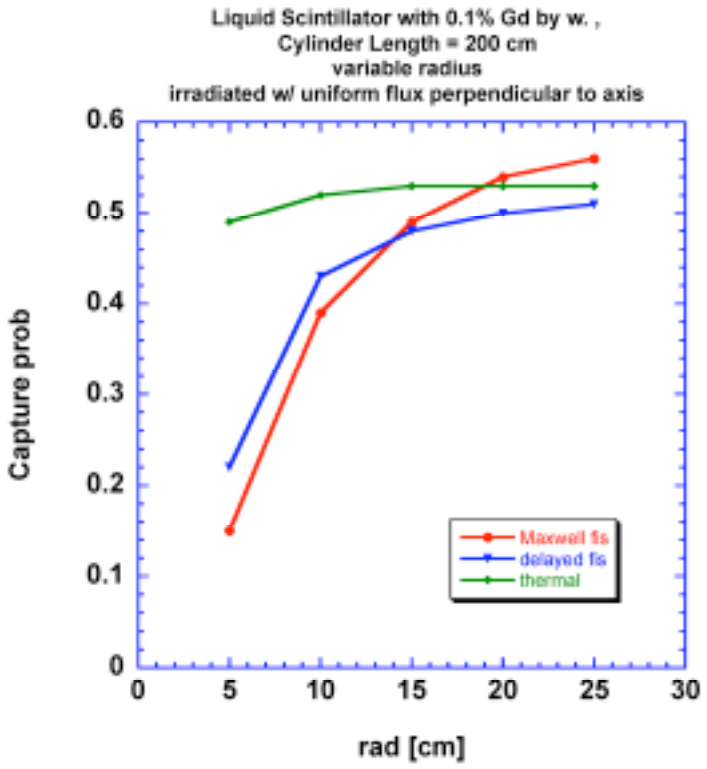

Figure 7.1.1 Detector array to detect signature SNM high-energy fission product □-rays.

We first did a feasibility study of the use of these detectors for our work. We performed Monte Carlo simulations of the neutron capture efficiency of Gd-loaded liquid scintillator. As seen in the figure below, the capture probability varies with the radius of the cylinder. We found that this detector would be an efficient detector for neutrons of any energy.

Figure 7.1.2 Monte Carlo simulations of capture efficiency of Gd-loaded scintillator.

Pictures of two small cells are shown below as well as a picture of the small cell alongside an unfilled standard cell.

Figure 7.1.3 Two small cells of the liquid scintillation detector

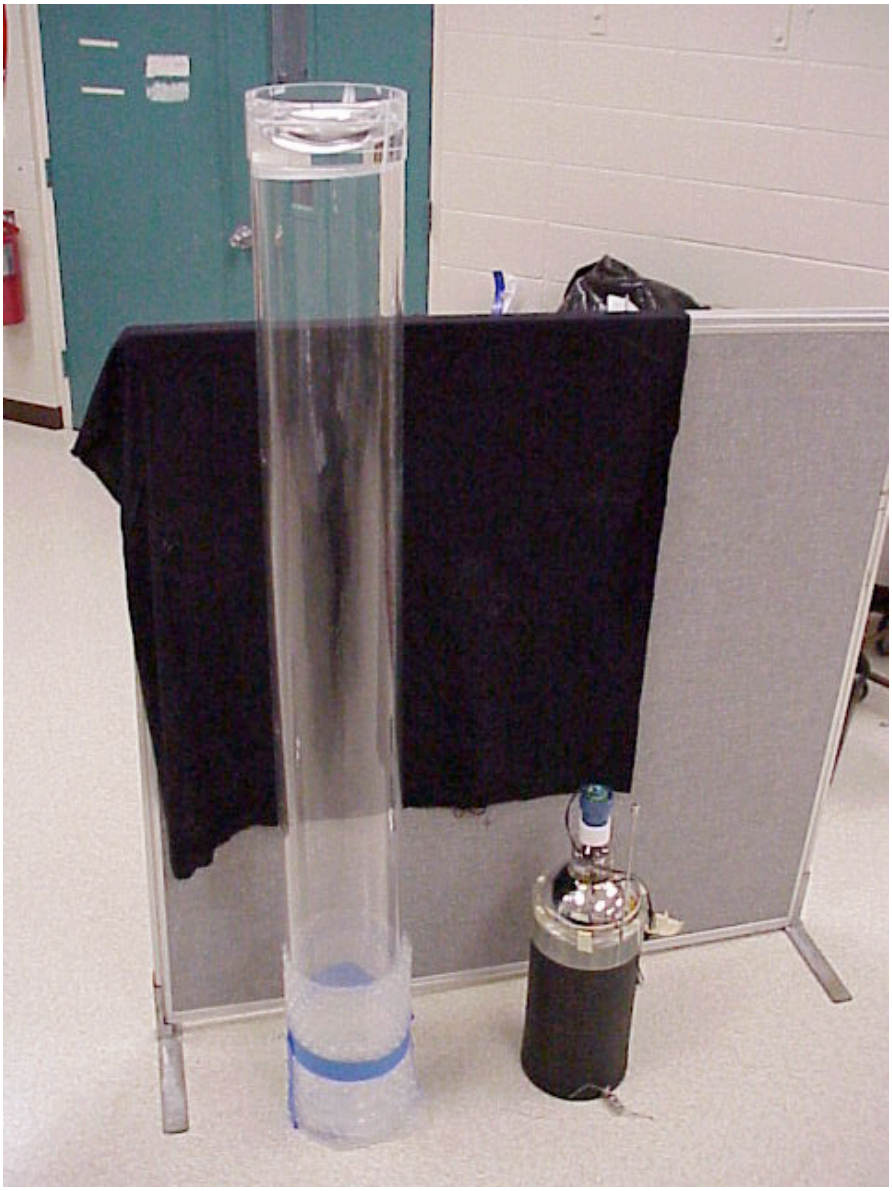

Figure 7.1.4 An unfilled standard scintillator cell alongside the small cell shown above

These detectors are estimated to have ~ 50% detection efficiency as an incident γ-ray undergoes multiple Compton scattering events in the large detector volume depositing much of its energy. An energy discriminator will be set to suppress response to any events depositing less than 3 MeV and that will reduce the detector efficiency to ~ 10%. A pulse height spectrum for one cell of this array is shown below where a ^{60}Co source illuminated the detector with its two γ-rays of equal intensity at 1.17 and 1.33 MeV.

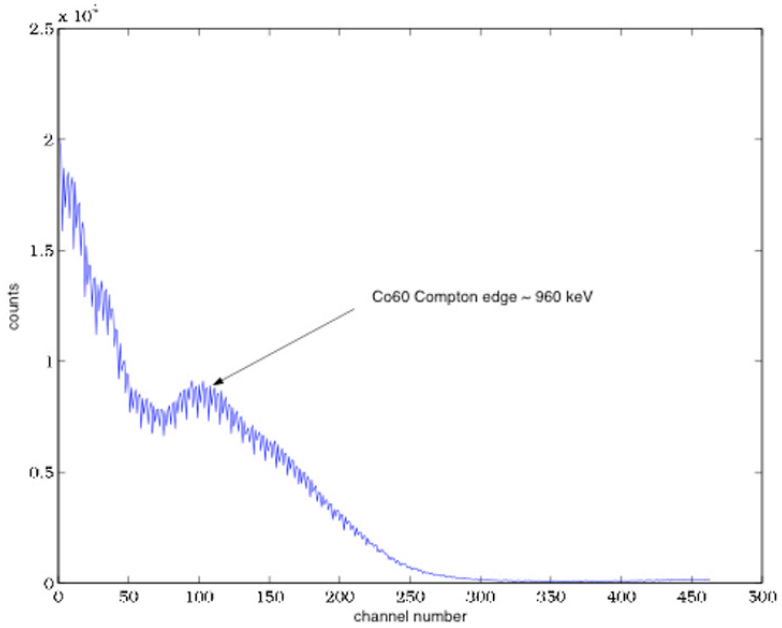

Figure 7.1.5 Pulse height spectrums from large liquid scintillator detector exposed to ^{60}Co γ-ray source.

Examination of the figure shows the resolution is very modest, but adequate to distinguish γ-rays separated by ~ 20% in energy. That capability will be adequate to discriminate signature fission product γ-rays at E_γ = 3-7 MeV from the low energy interferences. More importantly, these detectors have sufficiently high efficiency that the predicted signal strength of ~ 0.5 γ/cm^2/sec at the container wall will translate to 10^4 cps at the detectors.

The detector array has a relatively fast time resolution, ~ 100 ns or better, so that neutrons or γ-rays that are emitted as part of a fission chain can be identified from the multiplicity of events in the area at high count rates. This is an important capability that can detect significant neutron multiplication in an SNM assembly that would distinguish it clearly from legitimate cargo contents that may include natural uranium. The scintillators can detect fast neutrons from their scattering in the detector and also can detect thermal neutrons as they are captured in the Gd that is also loaded into the liquid scintillation material. The thermal neutron capture produces a very distinctive γ-ray cascade depositing a total of approximately ~ 8 MeV in the detector. Similarly, γ-rays emitted during fission chain events may lead to large multiplicity of γ-ray events in the array.

Since the array is subdivided into many elements forming pixels with dimensions ~ 30 cm, the acquired data contains information on the location of the target in the cargo container. As the induced radiation source scans along the detector array its position along the length of the container can be determined to within a few tens of cm.

Finally, the detector array can be used even if active neutron interrogation of the cargo is not called for. It can be used without the neutron source to scan for large amounts of radioactive material present in a cargo. The neutron and γ-ray sensitivity is very high so that small amounts of radioactivity can be detected. In addition, the array is segmented so that some indication of the

location or spatial extent of the radioactive material can be obtained from the count rates in multiple array elements. Establishing the geometrical extent of the radioactive material would help to distinguish a cargo with small amounts of uranium distributed throughout from the normal cargo with a small SNM component hidden in it.

8 Conclusions and prospects

The goal of the work reported here is to address the problem of detection of WMD materials within maritime containers. The problem is one of the most challenging facing the nation today.

We initially investigated the detection of chemical weapons and explosives using neutron activation. We performed simple signature measurements and simulations of gamma-ray spectra for several chemical simulants. We concluded that these simple approaches would require complex signal processing to identify these contraband materials in the presence of intervening materials found in cargo. We believe that simulations will be helpful in guiding this approach. Unfortunately, the nuclear data is inadequate in this region to perform detailed computations. Basic research is needed to fill in the cross section gaps for 14 MeV and lower neutron energies of many of the elements necessary for these simulations.

We concentrated on developing a concept for a neutron interrogation system that would detect small targets of fissile material, specifically 5 kg HEU or 1 kg Pu, even when well shielded by a thick cargo. It is essential that the concept be reliable and has low false-positive and false-negative error rates. It also must be rapid to avoid interruption of commerce. This concept was discussed in Section 2. A new radiation signature unique to fissile material has been identified that utilizes high-energy (E_{γ} = 3–7 MeV) fission product γ-radiation. First experiments were performed with our collaborators at LBNL to identify the abundance and characteristics of the new signature.

We used computational modeling to complement the experimental work. We used three-dimensional Monte Carlo simulation to simulate radiation flow. We described a dose estimation study in Section 3 that was used to help plan the laboratory design (Section 3). The study was compared to Health Physics measurements and agreed extremely well. In Section 4 we described more modeling work. We found the optimal arrangement of cargo simulant in our experiments, which helped our experimental planning. We predicted neutron and gamma fluences of delayed neutrons as a signature for the presence of HEU. We used modeling in the early design of the large liquid scintillation detectors, discussed in Section 7. The results helped verify the adequacy of the baseline flux of neutrons and photons into the detectors. The construction of the large cell detectors was nearly completed (except for final gluing) with LDRD funding. The testing was performed with follow-on NA22 funding.

Estimates of the characteristic spectrum of the fission product gamma radiation and intensity were presented in Section 5. Fortunately, this high-energy γ-ray signature is potentially robust in that it is very distinct compared to normal background radiation where there is no comparable high-energy γ-ray radiation. Equally important, this high-energy γ-ray signature has a higher yield than the classical delayed neutron technique and penetrates low-Z and high-Z cargos readily even at the greatest thickness expected. The ratio of the delayed

gammas to the delayed neutrons depends upon the gamma energy threshold. For 3 MeV the threshold radio is 8; for 4 MeV, the threshold is ~4. Consequently, the signature flux is at least 2-6 decades more intense than delayed neutron signals and facilitates the detection of fissile material even when shielded by thick cargos or when shielded intentionally. Characteristics of the new signature were predicted in Section 5 and we performed initial experiments to confirm this signature, described in Section 6.

These initial experiments revealed an important interference, namely the activation of ^{16}O to produce ^{16}N (by the $^{16}O(n,p)^{16}N$ reaction) to produce ^{16}N whose 7-sec β-decay produces a 6 MeV γ-ray. That interference is important when irradiating with 14 MeV neutrons but is eliminated when lower energy neutron sources are utilized, as its reaction threshold is 10 MeV. The predicted signature γ-ray fluxes exiting a thick cargo are relatively small as presented in Section 5; of order 1 $\gamma/cm^2/sec$. However, inexpensive and large arrays of scintillation detectors (described in Section 7) are relatively simple to deploy and these low fluxes then produce useful signal count rates of $2\text{-}4x10^4$ cps. That is high enough to quickly identify fissile material by its characteristic high-energy γ-radiation and characteristic short decay time, though the backgrounds in those detectors have not yet been determined. Experimental characterization of the γ-ray flux exiting thick cargos has not yet been undertaken. But the signature is expected to be robust and the γ-radiation only moderately attenuated in even the thickest cargos. The nominally 20-sec decay time of the SNM signature observed in the experiments is well matched to the ~ 1 minute goal for the time to scan a container.

A potentially viable concept for cargo interrogation has been presented and its components have been determined initially. Follow-on experimental work funded by DOE/NA-22 has confirmed this signature and will be reported elsewhere. This work has led to two patent applications at LBNL and LLNL. Utilization of the new γ-ray signature for fissile material appears to promise a dramatic improvement in sensitivity for those cases where thick intervening cargo shields a target of interest or where the material is shielded with intentionally placed high-Z materials. The work is currently funded by DHS, were experiments and simulations are in progress to quantitatively determine the effects of cargo or intentional shielding to reduce and/or interfere with the SNM signature. Those experiments will then be used to establish the scanning intervals required to reduce the error rates, i.e. false positive and false negative, to acceptable levels.

9 References

1. C. E. Grassley, M. Baucus, B. Thomas, C. B. Rangel, "Container security: Expansion of key customs programs will require greater attention to critical success factors ", General Accounting Office, US Congress, **GAO-03-770**, July 25, 2003, www.gao.gov/cgi-bin/getrpt?GAO-030770.

2. Maritime_Transport_Committee, "Security in maritime transport: Risk facators and economic impact ", Organization for Economic Co-operation and

Development (OECD); Directorate for Science, Technology and Industry, July, 2003, http://www.oecd.org/dataoecd/63/13/4375896.pdf.

3. M. M. May, D. Wilkening, T. L. Putnam, "Container security report", 2003, Center for International Security and Cooperation, http://cisac.stanford.edu/nuclearterrorism/index.html#3

4. PNL, "Nuclear and radiological threat detection for vehicle cargo ", Pacific Northwest National Laboratory, **PIET-43741-QR-005**, February 28, 2002,

5. S. Fetter, V. A. Frolov, M. Miller, R. Mozley, O. F. Prilutsky, S. N. Rodionov, R. Z. Sagdeev, "Detecting nuclear warheads", **Science & Global Security**, **1**, 1990, pp. 225-302.

6. J. Medalia, "Terrorist nuclear attacks on seaports: Threat and response", October 8, 2002, Personal communication.

7. NRC, Making the Nation Safer: The Role of Science and Technology in Countering Terrorism, The National Academies Press, Washington, DC (2002), pp.

8. LBNL_Nuclear_Science_Division, "Isotope Explorer", 2003, http://ie.lbl.gov/ensdf/

9. LBNL_Nuclear_Science_Division, "Table of Isotopes", 2003, Lawrence Berkeley National Laboratory, website, http://ie.lbl.gov/toi/

10. J. L. Jones, K. J. Haskell, J. M. Hoggan, D. R. Norman, W. Y. Yoon, "Photonuclear-based detection of nuclear smuggling in cargo containers", **Conference on Accelerator Applications in Research and Industry**, 12 November, 2002, Denton, TX,

11. J. L. Jones, W. Y. Toon, Y. D. Harker, J. M. Hoggan, K. J. Haskell, L. A. VanAusdein, "Proof-of-concept assessment of a photofission-based interrogation system for the detection of shielded nuclear material ", Idaho Nuclear Engineering Laboratory, **INEEL/EXT-2000-01523**, 2000,

12. G. R. Keepin, "Nuclear safeguards research and development ", Los Alamos National Laboratory, **LA-4368-MS**, October-December, 1969,

13. G. R. Keepin, "Nuclear safeguards research and development ", Los Alamos National Laboratory, **LA--4457-MS**, January-April, 1970,

14. LLNL_Nuclear_Data_Group, "Nuclear Data System 2000", 2003, http://www-ndg.llnl.gov/llnl/nds.cgi

15. H. Franz, W. Rudolph, H. Ohm, K. Kratz, G. Herrmann, F. Nuh, D. Slaughter, S. Prussin, "Delayed neutron spectroscopy with ^{3}He spectrometers", **Nuc. Inst. Meth. 144**, 253-261 (1977).

16. F. Nuh, D. Slaughter, S. Prussin, H. Ohm, W. Rudolph, K. Kratz, "Delayed neutrons and high energy □-rays from decay of ^{87}Br", **Nuc. Phys. A293**, 410-424 (1977).

17. M. P. Snell, "Gamma-ray technology: The practical container inspection alternative", 2001, SAIC, http://www.portechnology.org/,

18. R. D. Richardson, V. V. Verbinski, V. J. Orphan, "New cargo inspection and transportation technology applications", 2002, Port technology International, http://www.porttechnology.org/, May,

19. R. D. Richardson, V. V. Verbinski, V. J. Orphan, "New cargo inspection and transportation technology applications", 2001, SAIC, http://www.portechnology.org/,

20. C. J. McBee, D. W. Bowlin, V. J. Orphan, "Mobile cargo inspection provides improved throughput efficiency and flexibility", 2001, SAIC, http://www.portechnology.org/,

21. J. L. Jones, Y. D. Harker, W. Y. Yoon, L. O. Johnson, R. S. Lawrence, "Pulsed photon interrogation with neutron-induced gamma-ray spectrometry for cargo inspections", **Cargo Inspection Technologies**, **2276**, 326-338, 25-27 July, 1994, San Diego, CA, SPIE.

22. C. E. Moss, C. A. Goulding, C. L. Hollas, W. L. Myers, "Linear accelerator-based active interrogation for detection of highly enriched uranium", **Conference on Accelerator Applications in Research and Industry**, 12 November, 2002, Denton, TX,

23. J. Moss, D. Geesaman, L. Schroeder, J. Simon-Gillo, B. Keister, "Report on the workshop on the role of the nuclear physics research community in combating terrorism ", Department of Energy, **DoE/SC-0062**, 11-12 july, 2002,

24. E. B. Norman, S. G. Prussin, R.-M. Larimer, H. Shugart, E. Browne, A. R. Smith, R. J. McDonald, H. Nitsche, P. Gupta, M. I. Frank, T. B. Gosnell, "Signatures of special nuclear material: High-energy □-rays following fission ", Lawrence Livermore National Laboratory, **UCRL-JC-153259**, May, 2003,

25. R. A. Alvarez, A. D. Dougan, M. R. Rowland, T. F. Wang, "Neutron interrogation to identify chemical elements with an ion-tube neutron source (INS)", **J. Radioanal. Nucl. Chem 192**, 73-80 (1995).

26. W. C. Lee, D. B. Mahood, P. Ryge, P. Shea, T. Gozani, "Thermal neutron analysis (TNA) explosive detection based on electronic neutron generators", **Nuc. Inst. Meth. B 99**, 739-742 (1995).

27. A. P. Barzilov, P. C. Womble, G. Vourvopoulos, "NELIS - A neutron elemental inspection sysstem of commodities pallets", **2001 Office of National Drug Control Policy International Technology Symposium**, 2001,

28. D. R. Brown, T. Gozani, "Cargo inspection system based on pulsed fast neutron analysis", **Nuc. Inst. Meth. B 99**, 753-756 (1995).

29. D. R. Brown, "Cargo inspection system based on pulsed fast neutron analysis: an update", **Cargo Inspection Technologies**, **2276**, 449-456, 25-27 July, 1994, San Diego, CA, SPIE.

30. T. Gozani, "Understanding the physics limitations of PFNA - the nanosecond pulsed fast neutron analysis", **Nuc. Inst. Meth. B 99**, 743-747 (1995).

31. R. C. Smith, M. J. Hurwitz, K.-C. Tran, "System to detect contraband in cargo containers using fast and slow neutron irradition and collimated gamma detectors", **Nuc. Inst. Meth. B 99**, 733-735 (1995).

32. G. Vourvopoulos, P. C. Womble, "Pulsed fast/thermal neutron analysis: A technique for explosives detection", **TALANTA 54**, 459-468 (2001).

33. P. C. Womble, F. J. Schultz, G. Vourvopoulos, "Non-destructive characterization using pulsed fast-thermal neutrons", **Nuc. Inst. Meth. B 99**, 757-760 (1995).

34. P. Lebrun, P. Le Tourneur, B. Poumarede, H. Moller, P. Bach, "On-line analysis of bulk materials using pulsed neutron interrogation", **Application of Accelerators in Research and Industry**, **475**, 695-698, November, 1998, Denton, TX, American Institute of Physics.

35. P. C. Womble, C. Campbell, G. Vourvopoulos, J. Paschal, Z. Gacsi, S. Hui, "Detection of explosives with the PELAN system", **CP576, Application of Accelerators in Research and Industry-Sixteenth International Conference**, 0-7354-0015, 2001, American Institute of Physics.

36. P. C. Womble, G. Vourvopoulos, I. Novikov, J. Paschal, "PELAN 2001: Current status of the PELAN explosives detection system", **SPIE Conference on Hard X-ray and Gamma-ray Detector Physics**, July 29-August 3, 2001, San Diego, CA, Society of Photo-Optical Instrumentation Engineers.

37. P. C. Womble, G. Vourvopoulos, I. Novikov, J. Paschal, "PELAN 2001: Current status of the PELAN explosives detection system", **Hard X-ray and Gamma Ray Detector Physics**, 7/29-8/3, 2001, San Diego, CA, Society of Photo-Optical Instrumentation Engineers.

38. D. R. Brown, "Cargo inspection system based on pulsed fast neutron analysis", **SPIE 2092**, 254-262 (1993).

39. R. Loveman, J. Bendahan, T. Gozani, J. Stevenson, "Time of flight fast neutron radiography", **Nuc. Inst. Meth. B 99**, 765-768 (1995).

40. B. J. Micklich, C. L. Fink, T. J. Yule, "Key research issues in the pulsed fast-neutron analysis technique for cargo inspection", **Cargo Inspection Technologies**, **2276**, 310-320, 25-27 July, 1994, San Diego, CA, SPIE.

41. J. Bendahan, L. Feinstein, D. Keeley, R. Loveman, "Image reconstruction from pulsed fast neutron analysis", **Application of Accelerators in Research and Industry**, **475**, 726-730, November, 1998, Denton, TX, American Institute of Physics.

42. H. Martz, P. Griffin, "Assessment of cargo inspection technologies for the detection of explosives and drugs ", Lawrence Livermore National Laboratory, **FAA-191**, 2001,

43. S. M. Khan, "Review of neutron-based technologies for the inspection of cargo containers", **Cargo Inspection Technologies**, **2276**, 294-309, 25-27 July, 1994, San Diego, CA, SPIE.

44. M. Gmar, J. M. Capdevila, "Use of delayed gamma spectra for detection of actinides (U,Pu) by photofission", **Nuc. Inst. Meth. A 422**, 841-845 (2002).

45. LBNL_Nuclear_Science_Division, "Fission Home Page", 2003, http://ie.lbl.gov/fission.html

46. T. Rockwell III, Reactor Shielding Design Manual, D. Van Nostrand Co., New York (1956), pp.

47. H. Liskien, A. Paulsen, "Neutron production cross sections and energies for the reactions T(p,n)^{3}He, D(d,n)^{3}He and T(d,n)^{4}He", **Nuclear Data Tables 11**, 569-619 (1973).

48. L. C. Northcliffe, R. F. Schilling, "Range and stopping power tables for heavy ions", **Nuclear Data Tables A7**, 233-463 (1970).

49. T. S. Tenforde, L. L. Braby, L. Greenwood, C. B. Meinhold, S. D. Wiltshire, "Letter report on radiation protection advice for pulsed fast neutron analysis system used in security surveillance ", National Council on Radiation Protection and Measurements, **letter-**September 20, 2002,

50. Code of Federal Regulations, 21 CFR 179.26, (2003)

51. G. H. Pauli, "U. S. regulatory requirements for irradiating foods", 2001, Office of Premarket Approval, HFS-205, Center for Food Safety and Applied Nutrition, Food and Drug Administration, website, http://www.foodsafety.gov/~dms/opa-rdtk.html

52. Federal Register, 21 CFR 179, 62 FR 64108, (1997)

53. Code of Federal Regulations, 21 CFR 179, 66 FR 18537, (2001)

54. Code of Federal Regulations, 21 CFR 179.21, 440 (2003)

55. "Limitation of exposure to ionizing radiation ", National Council on Radiation Protection, **NCRP Report-116**, 1993

56. "Comparison of neutron instruments when exposed in the Bldg. 255 vault," Dale Hankins, memo to File, 2/10/02

57. "Survey results obtained in Bldg. 231," Dale Hankins, memo to File, 2/11/03

58. "Sulfur pellet counting," Dale Hankins, memo to File, 2/03

59. "Ratio of the 9/3-inch sphere and the thermal neutron dose rates from the ^{252} Cf neutron sources in Bldg. 255.

60. D. Slaughter, M. Accatino, A. Bernstein, J. Candy, A. Dougan, J. Hall, A. Loshak, D. Manatt, A. Meyer, B. Pohl, S. Prussin, R. Walling, D. Weirup, "Detection of special nuclear material in cargo containers using neutron interrogation", UCRL-ID-155315, August 2003.

61. D. Slaughter, M. R. Accatino, A. Bernstein, A.D. Dougan, J. M. Hall, A. Loshak, D. R. Manatt, B.A. Pohl, S.G. Prussin, R. S. Walling, D. L. Weirup, UCRL-JRNL-202106, submitted to IEEE Sensors Journal, January 2004.

62. J. Briemeister, Ed., "MCNP-A General Monte Carlo N-ParticleTransport Code, Version 4C" Report LA-13709-M, Los Alamos National Laboratory, Los Alamos, New Mexico (2000).

63. R. Buck, "COG User's Manual, A Multiparticle Monte Carlo Transport Code," LLNL, 5th Edition, v. 10. (review in process - 2004).